AD-P001 605

COMPONENT PART NOTICE

THIS PAPER IS A COMPONENT PART OF THE FOLLOWING COMPILATION REPORT:

(TITLE): Behaviour of Short Cracks in Airframe Components, Conference Proceedings of the Meeting of the AGARD Structures and Materials Panel (55th) Held at Toronto, Canada on 19-24 September 1982.

(SOURCE): Advisory Group for Aerospace Research and Development, Neuilly-sur-Seine (France).

TO ORDER THE COMPLETE COMPILATION REPORT USE AD-A131 159.

THE COMPONENT PART IS PROVIDED HERE TO ALLOW USERS ACCESS TO INDIVIDUALLY AUTHORED SECTIONS OF PROCEEDINGS, ANNALS, SYMPOSIA, ETC. HOWEVER, THE COMPONENT SHOULD BE CONSIDERED WITHIN THE CONTEXT OF THE OVERALL COMPILATION REPORT AND NOT AS A STAND-ALONE TECHNICAL REPORT.

THE FOLLOWING COMPONENT PART NUMBERS COMPRISE THE COMPILATION REPORT:

AD#:		TITLE:
	P001 602	Mechanics and Physics of the Growth of Small Cracks.
	P001 603	Fatigue Damage Mechanisms and Short Crack Growth.
	P001 604	An Assessment of the Importance of Small Crack Growth to Aircraft Design.
	P001 605	A Nonlinear Fracture Mechanics Approach to the Growth of Small Cracks.
	P001 606	Damage Tolerance Evaluation of Structures with Small Cracks.
	P001 607	Fracture Mechanics Analysis of Short Cracks at Loaded Holes.
	P001 608	Probabilistic Fracture Mechanics Analysis Methods for Structural Durability.
	P001 609	The Effects of Compressive Overloads on the Threshold Stress Intensity for Short Cracks.
	P001 610	Crack Propagation at Short Crack Lengths under Variable Amplitude Loading (2nd Report).
	P001 611	Spectrum Effects on the Growth of Short Cracks.
	P001 612	A Study of Small Crack Growth under Transport Spectrum Loading.
	P001 613	Small Cracks in Large Forgings.
	P001 614	'Short Crack' Fatigue Design Considerations: Modelling, Characterisation Interpretation, Detection: Prediction of Behavior.

DISCLAIMER NOTICE

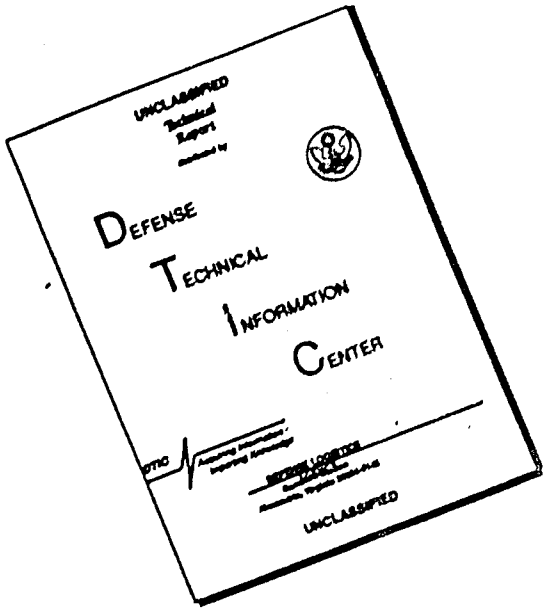

THIS DOCUMENT IS BEST QUALITY AVAILABLE. THE COPY FURNISHED TO DTIC CONTAINED A SIGNIFICANT NUMBER OF PAGES WHICH DO NOT REPRODUCE LEGIBLY.

6-1

A NONLINEAR FRACTURE MECHANICS APPROACH TO THE GROWTH OF SMALL CRACKS

J. C. Newman, Jr.
NASA Langley Research Center
Hampton, Virginia 23665, U.S.A.

AD-P001 605

SUMMARY

Using linear-elastic and nonlinear fracture mechanics, many investigators have tried to explain the growth of small cracks in plates and at notches. These studies have concentrated on the growth of small cracks ranging in length from 10^{-2} to 1 mm. On the basis of linear-elastic fracture mechanics, the small cracks grew much faster than would be predicted from large crack data. Nonlinear fracture mechanics, in particular the J-integral concept, and an empirical length parameter have been used to correlate small and large crack-growth rate data. The physical interpretation of the length parameter, however, is unclear.

Recently, some investigators have suggested that crack closure may be a major factor in causing differences between growth of small and large cracks. The purpose of the present paper is to use an analytical model of crack closure to study the crack growth and closure behavior of small cracks in plates and at notches. The calculated crack-opening stresses for small and large cracks, together with elastic and elastic-plastic fracture mechanics analyses, are used to correlate crack-growth rate data. At equivalent elastic stress-intensity factor levels, calculations predict that small cracks in plates and at notches should grow faster than large cracks because the applied stress needed to open a small crack is less than that needed to open a large crack. These predictions agree with observed trends in test data. The calculations from the model also imply that many of the stress-intensity factor thresholds that have been developed in tests with large cracks and with load-reduction schemes do not apply to the growth of small cracks.

The current calculations are based upon continuum mechanics principles and, thus, some crack size and grain structure exist where the underlying fracture mechanics assumptions become invalid because of material inhomogeneity (grains, inclusions, etc.). Admittedly, much more effort is needed to develop the mechanics of a noncontinuum. Nevertheless, these results indicate the importance of crack closure in predicting the growth of small cracks from large crack data.

NOMENCLATURE

A_k	coefficients in stress-intensity factor equation (k = 1,2)
b	location of concentrated force, m
b_k	dimensions for partially-loaded crack (k = 1,2), m
c	half length of crack, m
c_i	half length of initial crack in load-reduction scheme, m
c_n	half length of crack-starter notch, m
d	half length of crack plus tensile plastic zone, m
E	Young's modulus of elasticity, MPa
F	boundary-correction factor on stress-intensity factor
K	stress-intensity factor, MPa-$m^{1/2}$
N	number of cycles
n	number of bar elements in crack-closure model
P	applied load, N
P_i	applied load at initiation of load-reduction scheme, N
P_{max}	maximum applied load, N
P_o	crack-opening load, N
R	stress ratio (S_{min}/S_{max})
r	radius of circular hole, m
S	applied stress, MPa

S_c	crack-closure stress, MPa
S_i	applied stress at initiation of load-reduction scheme, MPa
S_{max}	maximum applied stress, MPa
S_{min}	minimum applied stress, MPa
S_o	crack-opening stress, MPa
t	specimen thickness, m
V	crack-surface displacement, m
V_c	displacement of crack-tip element, m
w	half width of specimen, m
w_j	half width of bar element at point j, m
x,y	Cartesian coordinates
x_i	coordinate location of element i, m
α	constraint factor, $\alpha = 1$ for plane stress and $\alpha = 3$ for plane strain
ΔK	stress-intensity factor range, MPa-$m^{1/2}$
ΔK_{eff}	effective stress-intensity factor range, MPa-$m^{1/2}$
$\Delta \bar{K}_{eff}$	plastic-zone corrected effective stress-intensity factor range, MPa-$m^{1/2}$
ΔK_{th}	threshold stress-intensity factor range, MPa-$m^{1/2}$
ΔS_{eff}	effective stress range, MPa
η	material constant, $\eta = 0$ for plane stress and $\eta = \nu$ for plane strain
ν	Poisson's ratio
ρ	length of tensile plastic zone, m
σ_j	stress on segment of crack surface, MPa
σ_o	flow stress, MPa
σ_u	ultimate tensile strength, MPa
σ_{ys}	yield stress (0.2 percent offset), MPa
ω	length of compressive plastic zone, m

INTRODUCTION

Most experimental and analytical studies on fatigue-crack growth have been conducted on "large" cracks with lengths in excess of 2 mm. However, in many engineering structures, crack growth from "small" pre-existing flaws is a major portion of the component's fatigue life. Numerous investigators [1-11] have observed that the growth characteristics of small fatigue cracks in plates and at notches differ from those of large cracks in the same material. These studies have concentrated on the growth of small cracks ranging in length from 10^{-2} to 1 mm. On the basis of linear-elastic fracture mechanics (LEFM), the small cracks grew much faster than would be predicted from large crack data. This behavior is illustrated in Figure 1, where the crack-growth rate is plotted against the linear-elastic stress-intensity factor range, ΔK. The solid (sigmoidal) curve shows a typical result for a given material and environment under constant-amplitude loading. The solid curve is usually obtained from tests with large cracks. At low growth rates, the threshold stress-intensity factor range, ΔK_{th}, is usually obtained from load-reduction (K-decreasing) tests. Some typical experimental results for small cracks in plates and at notches are shown by the dashed curves. These results show that small cracks grow faster than large cracks at the same ΔK level and that they also grow at ΔK levels below threshold.

Using nonlinear fracture mechanics, some investigators have tried to explain the growth of small cracks in plates and at notches. In particular, the J-integral concept and an empirical length parameter [3,4] have been used to correlate small-crack and large-crack growth rate data. The physical interpretation of the length parameter, however, is unclear. More recently, several investigators [5-11] have suggested that crack closure [12,13] may be a major factor in causing the differences between the growth of small and large cracks.

6.3

Many of the comparisons between growth rates for small and large cracks have been made in the low crack-growth rate region associated with threshold (ΔK_{th}) for large cracks. Measurement of ΔK_{th}, using load-reduction schemes [14-17], establishes a regime of crack sizes and applied stress levels where crack growth would not occur. But small cracks and cracks from pre-existing flaws have been observed to grow [1-3,10] at stress-intensity factor levels below ΔK_{th}, as shown in Figure 1. Here again, several investigators [18-20] have experimentally shown that crack closure is causing the stress-intensity factor threshold under load-reduction schemes. On the basis of these results, an important question concerning the growth of large cracks at extremely low stress levels arises. Is the ΔK-rate relationship for large cracks under constant-amplitude loading given by the dash-dot curve in Figure 1? Admittedly, a threshold could exist for large cracks due to material inhomogeneities and environmental factors, such as oxide or corrosion products on the crack surfaces [21,22]. But these thresholds must be obtained in tests without any load-interaction effects.

To adequately resolve the differences between the growth of small and large cracks, crack-closure effects must be considered. This paper is concerned with the analytical treatment of crack closure. A simple strip-yield model of crack closure was developed in Reference 23, but a more useful model was developed in References 24 and 25. There have also been several other attempts to develop simple analytical models of crack closure, but a review here is beyond the scope of the present paper (see Ref. 25).

The purpose of the present paper is to use an analytical closure model [25] to study the crack growth and closure behavior of small cracks in plates and at holes, and to study the closure behavior of large cracks under load-reduction schemes used in threshold testing. The model used here simulates the influence of plane-stress and plane-strain conditions on yielding at the crack tip. The model is based on the Dugdale model [26], but modified to leave plastically deformed material along the crack surfaces as the crack grows. Two configurations are analyzed: (1) a center-crack tension specimen and (2) two symmetric cracks emanating from a circular hole. A surface-crack configuration is also considered, but it is analyzed as a center-crack specimen with a modified stress-intensity factor solution. The crack-opening stresses for these configurations are calculated as a function of crack length for constant-amplitude loading and for the load-reduction schemes used for threshold testing. An improved method of calculating crack-opening stresses, using crack-surface displacements, is also presented. The calculated crack-opening stresses are compared with experimental measurements made under a load-reduction scheme.

Because specimens with small cracks are usually subjected to high stress levels, Elber's effective stress-intensity factor range [13] is modified herein for plasticity. Crack-growth rates under constant-amplitude loading are correlated with the plastic-zone corrected effective stress-intensity factor range, $\Delta \bar{K}_{eff}$, over a wide range of stress ratios. Using the crack-growth rate and $\Delta \bar{K}_{eff}$ correlations for large cracks in several materials, predicted growth rates for small cracks in plates and at circular holes are compared with experimental rates.

FATIGUE CRACK-CLOSURE ANALYSIS

The following sections include a brief description of the analytical crack-closure model [25] and of the assumptions made in the application of the model to the growth of small cracks. These sections also include a description of the plastic-zone corrected effective stress-intensity factor range and its correlation with crack-growth rates.

Analytical Crack-Closure Model

To calculate crack-closure and crack-opening stress during fatigue crack growth, the elastic-plastic solution for stresses and displacements in a cracked body must be known. Because there are no closed-form solutions to elastic-plastic cracked bodies, simple approximations must be used when finite-element solutions [23] are inappropriate. The Dugdale model [26] is one such approximation. The crack-surface displacements, which are used to calculate contact (or closure) stresses under cyclic loading, are influenced by plastic yielding at the crack tip and residual deformations left in the wake of the growing crack. The applied stress level at which the crack surfaces become fully open (no surface contact) is directly related to contact stresses.

The analytical closure model developed in Reference 25 is for a central crack in a finite-width specimen subjected to uniform applied stress (Fig. 2(a)). This model is extended herein to cracks emanating from a circular hole in a finite-width specimen subjected to uniform applied stress (Fig. 2(b)). The model is based on the Dugdale model, but modified to leave plastically deformed material in the wake of the crack. The primary advantage in using this model is that the plastic-zone size and crack-surface displacements are obtained by superposition of two elastic problems--a crack in a plate subjected to a remote uniform stress, S, or to a uniform stress, σ, applied over a segment of the crack surface. The stress-intensity factor and crack-surface displacement equations for these loading conditions on a plate with a central crack are given in Reference 25. The corresponding equations for cracks emanating from a circular hole are given in Appendix A.

Figure 3 shows a schematic of the model at maximum and minimum applied stress. The model is composed of three regions: (1) a linear-elastic region containing a circular hole with a fictitious crack of half-length $c + \rho$, (2) a plastic region of length ρ,

and (3) a residual plastic deformation region along the crack surface. The physical crack is of length $c - r$, where r is the radius of the circular hole. The compressive plastic zone is ω. Region 1 is treated as an elastic continuum; the crack-surface displacements under various loading conditions are given in Reference 25 for a central crack and in Appendix A for cracks emanating from a hole. Regions 2 and 3 are composed of rigid-perfectly plastic (constant stress) bar elements with a flow stress, σ_o. The flow stress is taken as the ultimate tensile strength (σ_u) herein because some tests were conducted at very high applied stress levels. (If a nonlinear stress-strain curve had been incorporated into the model [27], the need for an assumed flow stress would have been eliminated.) The shaded regions in Figures 3(a) and 3(b) indicate material that is in a plastic state. At any applied stress level, the bar elements are either intact (in the plastic zone) or broken (residual plastic deformation). The broken elements carry compressive loads only, and then only if they are in contact. The elements yield in compression when the contact stress reaches $-\sigma_o$. Those elements that are not in contact do not affect the calculation of crack-surface displacements. To account for the effects of state of stress on plastic-zone size, a constraint factor α was used to elevate the tensile flow stress for the intact elements in the plastic zone. The effective flow stress $\alpha\sigma_o$ under simulated plane-stress conditions was σ_o and under simulated plane-strain conditions was $3\sigma_o$. The constraint factor is a lower bound for plane stress and an approximate upper bound for plane strain [25]. The constraint factor was assumed to be 1, 1.73 (Irwin's plane-strain constraint [28]), or 3, depending upon the test conditions. Plane-stress conditions were assumed for high applied stress levels and for crack-growth rates higher than the rate at transition (flat to slant crack growth) [29] because the plastic-zone size would be of the order of the plate thickness. Plane-strain conditions were assumed for crack-growth rates lower than the rate at transition because the plastic-zone size would be small compared to plate thickness. Where the constraint conditions were unknown, such as a small surface crack, plane-stress and plane-strain conditions were both tried.

The analytical closure model was used to calculate crack-opening stresses as a function of crack length and load history. The applied stress level at which the crack surfaces are fully open is denoted as S_o, the crack-opening stress. These stresses have been calculated by two methods. One method was based on the stress-intensity factor due to contact stresses at the minimum applied stress; the other was based on crack-surface displacements. Under constant-amplitude loading, the crack closes first and opens last at the crack tip, so the stress-intensity factor method was used to calculate S_o [24,25]. However, under some variable-amplitude loading conditions and the load-reduction schemes used for threshold testing, the crack closes first and opens last away from the tip. Under these conditions, the stress-intensity factor method was inadequate. The crack-surface displacement method was more accurate in calculating the applied stress level at which the crack surfaces open completely under general cyclic loading. In this paper, the displacement method was used to calculate S_o and is presented in Appendix B.

The closure model was only used to calculate crack-opening stresses. In turn, the crack-opening stress was used to calculate the plastic-zone corrected effective stress-intensity factor range and then the crack-growth rate.

Plastic-Zone Corrected Effective Stress-Intensity Factor Range

Elber's effective stress-intensity factor range [13] is based on linear-elastic stress-intensity factors. For small cracks and high stress levels, the plastic-zone sizes are no longer small compared to crack size, and linear-elastic analyses are inadequate. To correct the analyses for plasticity, the Dugdale plastic-zone length (ρ) is added to crack length (c), like Irwin's plastic-zone correction [28]. Thus, the plastic-zone corrected stress-intensity factor range is

$$\Delta\bar{K} = (S_{max} - S_{min}) \sqrt{\pi d}\, F\left(\frac{r}{d}, \frac{r}{w}, \frac{d}{w}\right) \qquad (1)$$

where $d = c + \rho$ and ρ is calculated at the maximum applied stress, S_{max}, using the equations given in Appendix C. The boundary-correction factor F accounts for the influence of hole radius and specimen width, and is given by the product of the functions F_h^s and F_w^s. These functions are given in Appendix A, by Eqs. (6) and (22), respectively. (This parameter, $\Delta\bar{K}$, is similar to Barenblatt's cohesive modulus [30] under cyclic loading.)

The plastic-zone corrected effective stress-intensity factor range was obtained from Eq. (1) by replacing S_{min} by S_o, like Elber's modification, and is given by

$$\Delta\bar{K}_{eff} = U\,\Delta\bar{K} = \frac{S_{max} - S_o}{S_{max} - S_{min}}\,\Delta\bar{K} \qquad (2)$$

Fatigue Crack Growth Rates

Instead of using an equation to relate the crack-growth rates to $\Delta\bar{K}_{eff}$, a table-lookup procedure was used in this paper. The primary advantage in using a table is that the baseline crack-growth rate data can be described more accurately than with a

multi-parameter equation, especially in the transitional region (flat to slant crack growth). To illustrate the construction and use of the table, an example is shown.

Center-crack tension (CCT) specimens (w = 80 mm) were used to obtain crack-growth rate data on 2024-T3 Alclad aluminum alloy sheet (t = 2 mm) material [5]. The tensile strength (σ_u) and the assumed flow stress (σ_o) of the material were 475 MPa. The maximum applied stress level S_{max} was 77.5 MPa at an R ratio of 0.01. A plot of log dc/dN against log ΔK was constructed. The ΔK values at selected crack-growth rates are listed in the following table:

$\frac{dc}{dN}$, mm/cycle	ΔK, MPa-$m^{1/2}$	$\Delta\bar{K}$, MPa-$m^{1/2}$	$\frac{S_o}{S_{max}}$	$\Delta\bar{K}_{eff}$, MPa-$m^{1/2}$
7.6E-06	6.59	6.70	0.571	2.90
3.0E-05	8.79	8.95	.596	3.65
4.3E-05	12.64	12.86	.597	5.23
6.8E-05	14.29	14.58	.596	5.95
1.2E-04	17.58	18.06	.600	7.30
3.8E-04	19.78	20.20	.599	8.18
1.3E-03	25.28	25.88	.594	10.61
7.6E-03	36.27	38.25	.578	16.30

The rates were selected so that straight lines between each adjacent data point would describe the ΔK-rate data using a visual fit.

Next, the plastic-zone corrected stress-intensity factor, $\Delta\bar{K}$, was computed from Eq. (1) with the plastic-zone size given by Eq. (31). The constraint factor (α) was assumed to be unity because most of the data had rates higher than the rate at transition (about 3×10^{-5} mm/cycle). For small ΔK levels, $\Delta\bar{K}$ is given approximately by

$$\Delta\bar{K} \approx \Delta K \sqrt{\sec\left(\frac{\pi S_{max}}{2\alpha\sigma_o}\right)} \tag{3}$$

A closure analysis was then conducted on a CCT specimen subjected to a maximum applied stress (S_{max}) of 77.5 MPa with an R ratio of 0.01. The initial crack length was 1.5 mm. Crack-opening stresses were calculated as a function of crack length from the model. The crack-opening stress for each value of ΔK is listed in the table. Values of $\Delta\bar{K}_{eff}$ were computed from Eq. (2). The table of dc/dN against $\Delta\bar{K}_{eff}$ forms the crack-growth rate data used in all predictions made on this material and thickness. The crack-growth rates at intermediate values of $\Delta\bar{K}_{eff}$ were obtained by assuming a power-law equation, $C_1 \Delta\bar{K}_{eff}^{C_2}$, between the two adjacent data points. For $\Delta\bar{K}_{eff}$ values outside of the table, the power-law equation between the two closest data points was extrapolated.

APPLICATION OF THE CRACK-CLOSURE ANALYSIS

The analytical closure model is used to calculate crack-opening stresses under constant-amplitude loading and under the load-reduction schemes used for threshold testing. Some comparisons are made between calculated and experimental crack-opening stresses for these loading conditions on a steel and an aluminum alloy.

Crack-growth rates under constant-amplitude loading for large cracks (c > 2 mm) in a steel, an aluminum alloy, and a cast (nickel-aluminum-bronze) alloy are correlated with the plastic-zone corrected effective stress-intensity factor range. Using these correlations, the growth rates for small cracks in plates or at circular holes are predicted and compared with experimental growth rates.

Constant-Amplitude Loading

To show how the crack-opening stress influences the local crack-tip displacements under constant-amplitude loading, and consequently the crack-tip damage or crack growth, the applied stress (S) is plotted against the displacement (V_c) of the crack-tip element in Figure 4. The maximum applied stress was $0.4\sigma_o$ and the specimen was cycled at an R ratio of zero. Recalling that the elements in the plastic zone are rigid-perfectly plastic, no change in displacement occurs until the element yields. The calculated crack-opening stress from the displacement method (Appendix B) is shown as the solid symbol on the loading branch. These results demonstrate the significance of crack closure, in that all cyclic loads below S_o would cause no plastic deformation at the crack tip and, presumably, no crack growth. These results also show that the crack opens before the crack-tip element yields. This was caused by the finite stress concentration

6-6 in the model (elastic stress concentration was about 30). If the model had had an infinite stress concentration, like an ideal crack, then the element would have yielded when the crack tip opened. Likewise, compressive yielding occurred only after some unloading. The crack-closure stress (S_c) is shown as the solid symbol on the unloading branch. S_c is the stress level at which the first crack-surface element at the crack tip closes. In this example, the crack was not allowed to grow during the loading branch. If the crack had been allowed to grow, then closure would have occurred over the newly created crack surface after a smaller amount of unloading.

The closure model was exercised under simulated plane-stress and plane-strain conditions for constant-amplitude loading. The calculated S_o values for the CCT specimen remained nearly constant over a very wide range of crack lengths [25]. This constant value is called the "stabilized" crack-opening stress. The stabilized crack-opening stresses, normalized by S_{max}, are plotted against stress ratio for various stress levels in Figure 5. The calculations were made on CCT specimens made of an aluminum alloy, but the results also apply for steels and titanium alloys when the material behavior is elastic-perfectly plastic. At any R ratio, the S_o/S_{max} values are lower for higher values of α and for higher values of stress level (S_{max}/σ_o). The influence of stress level was more pronounced under plane-stress conditions (solid curves) than under plane-strain conditions (dashed curves).

Threshold Testing

Because many of the comparisons between the growth of small and large cracks have been made in the crack-growth rate region associated with thresholds for large cracks, it is important to know whether the threshold is a material behavior or is caused by the load-reduction scheme. Some load-reduction schemes used to obtain ΔK_{th} are shown in Figure 6. The ratio of current load (or stress) to the initial load (or stress) is plotted against crack length. The crack length at initiation of the load-reduction scheme was 20 mm in a CCT specimen (w = 100 mm). The solid curve from Bucci [17] (proposed ASTM test method) is based on a constant rate of change in normalized plastic-zone size with crack extension and is independent of the R ratio. The normalized K-gradient, $(dK/dc)/K$, was $-0.08\ mm^{-1}$, as recommended. The dashed curves show the load-reduction scheme proposed by Ohta et al. [19] for R = 0 and 0.8. Their scheme is based on a constant ΔK-gradient, $d(\Delta K)/dc$. The ΔK-gradient ranged from -20 to -100 $MPa/mm^{1/2}$. The smallest ΔK-gradient was used in Figure 6. The step function was proposed by Robin and Pluvinage [16]. The load was reduced by 10 percent after 0.2 mm of crack extension. The crack extension was large enough for the crack to traverse the plastic zone created by the previous load.

As previously mentioned, several investigators [18-20] have experimentally shown that the stress-intensity factor threshold under load-reduction schemes can be explained by the crack-closure behavior. Some typical results on an aluminum alloy are shown in Figure 7. Minakawa and McEvily [31] conducted a threshold test on a compact specimen and measured the crack-opening loads as the ΔK level approached ΔK_{th}. The crack-opening loads were determined from a displacement gage at the edge of the compact specimen. This location was remote from the crack tip. For high ΔK levels, the P_o/P_{max} values ranged from 0.15 to 0.35. The horizontal line is the calculated P_o/P_{max} ratio from the closure model under constant-amplitude loading with plane-strain conditions (α = 3). The calculated ratio agreed fairly well with the experimental values. As ΔK approached ΔK_{th}, the P_o/P_{max} ratio rapidly rose and the ratio was nearly unity at threshold. Thus, the rise in crack-opening load explains why the threshold developed. But what caused the rise in crack-opening loads? A number of suggestions have been advanced to explain this behavior. Among these are the mismatch of crack-surface features observed by Walker and Beevers [32] in a titanium alloy; the corrosion product formation on the crack surfaces, as observed by Paris et al. [33] and Ritchie et al. [34]; and the variation in the mode of crack growth with stress-intensity factor level as reported by Ohtsuka et al. [35], and Minakawa and McEvily [31]. The mismatch of crack-surface features and corrosion products on the crack surfaces could cause the surfaces to come into contact at a higher load than the load for a crack without the mismatch or corrosion products. The mode of crack growth near threshold is a combination of Mode I and Mode II (tensile and shear) instead of pure Mode I. The mixed-mode crack growth causes an irregular crack surface profile and, consequently, the possibility of crack-surface mismatch. The analytical treatment of crack closure due to crack-surface mismatch or corrosion products on the crack surface is beyond the scope of the present paper.

However, now consider the influence of the load-reduction scheme on crack closure. Using the closure model, a simulated threshold test was conducted on a CCT specimen made of steel using Bucci's load-reduction scheme [17]. The material flow stress was 800 MPa and the constraint factor was assumed to be unity. The applied load (or applied stress) against crack length is shown by the solid curve in Figure 6 at an R ratio of zero. The crack length at initiation of the load-reduction scheme (c_i) was 20 mm. As the applied stress was reduced with crack extension, the closure model predicted a rise in crack-opening stress. To find out why the crack-opening stress rose, the crack-tip displacements during a single cycle are shown in Figure 8. The figure shows applied stress normalized by the maximum applied stress plotted against displacement of the crack-tip element, similar to that shown in Figure 4 for constant-amplitude loading. Again, the crack-opening stress is shown by the solid symbol on the loading branch. Here, the crack-opening stress is higher than the value calculated for constant-amplitude loading (shown by the dashed line). In contrast to the closure behavior under constant-amplitude loading, in the threshold test the crack did not close near the crack tip but did close

away from the crack tip, as illustrated in the insert. The insert shows a schematic of the crack-surface displacements near threshold. The shaded region around the crack depicts the residual plastic deformations left in the wake of the growing crack. The largest residual deformations occur along the crack at about c_i and, consequently, the crack-opening stress is controlled by the displacements in this region. These displacements tend to prop the crack open at the tip. Figure 8 shows that the crack-tip element does not change in displacement until after the crack surfaces are fully open. During unloading, S_c' shows the applied stress level at which the crack surfaces close away from the tip and S_c shows the applied stress level at which the crack tip closes.

Ohta et al. [19] tested CCT specimens made of HT80 steel (t = 10 mm) over a wide range of R ratios (-1 to 0.8) to determine crack-growth rates down to threshold and to measure crack-opening stresses. They used the Ohta-Sasaki load-reduction scheme (dashed curves shown in Fig. 6) and a small crack-tip displacement gage to measure S_o values. Some typical results on crack-opening stresses for R = 0 are shown in Figure 9. The S_o/S_{max} ratio is plotted against ΔK level during the load-reduction scheme. The crack-opening ratio was constant down to a ΔK level of about 15 MPa-$m^{1/2}$. Near this level, the ratio rapidly rose as the applied loads were reduced and a threshold developed at about 7 MPa-$m^{1/2}$. The solid curves show calculations from the closure model with α = 1 and 1.73. The plane-stress calculations are in good agreement with the experimental data down near threshold. Because their crack-closure measurements were made on the surface of the specimen, their results should be close to those for plane-stress conditions. Similar comparisons at R = 0.8 and -1 show similar agreement between plane-stress calculations and measurements (not shown).

But crack closure near the free surfaces of a specimen may not control the overall growth rate through the thickness of a specimen. In fact, the crack-opening stresses vary through the thickness of a specimen [36]. Thus, the overall growth rate at low ΔK values may be controlled by a higher constraint factor than that of plane stress. To determine the proper constraint factor, a three-dimensional analysis would be required. However, the correlation of crack-growth rate data at various stress ratios could also be used to experimentally determine an approximate constraint factor [37]. Using a plot of ΔK and rate for various R ratios, as shown in Figure 10(a) for the HT80 steel, the spread in the data as a function of R can be used to find the crack-opening stresses needed to correlate the R-ratio data on a $\Delta\bar{K}_{eff}$ and rate plot. Because crack-opening stresses are a function of constraint factor (see Fig. 5), an approximate constraint factor can be found to correlate the data. For the 10-mm-thick steel specimens at low ΔK levels, plane-strain conditions were expected to exist under constant-amplitude loading. Figure 10(b) shows a plot of $\Delta\bar{K}_{eff}$ and rate for the same HT80 steel data using a closure analysis under plane-strain conditions (α = 3). Curves were drawn through the data for each R ratio. Growth rates above 5 x 10^{-6} mm/cycle, basically generated under constant-amplitude loading, correlated quite well under plane-strain conditions even for high ΔK values. But the threshold data showed systematic variations with $\Delta\bar{K}_{eff}$. Recalling how well the closure analysis under plane-stress conditions (α = 1) predicted threshold behavior under a load-reduction scheme (see Fig. 9), the growth rate data on the HT80 steel were replotted in Figure 11 using a closure analysis with α = 1 (Fig. 11(a)) and α = 3 (same as Fig. 10(b)). These results show that plane-stress closure is controlling the growth rates near threshold under a load-reduction scheme.

Apparently, the plane-stress regions near the free surfaces of a specimen play an important role on crack-closure effects under load-reduction schemes and variable-amplitude loading. McEvily [38] conducted experiments to confirm the importance of crack closure near the free surfaces. He found, in a test on a 6061 aluminum alloy specimen (t = 12.7 mm), that a spike load caused significant crack-growth delay. In a second test, he carefully machined 25 percent of the thickness from each surface of the specimen after the application of the spike load and found very little crack-growth delay. Thus, the crack-closure effect under spike loading is predominantly a surface phenomenon.

As shown by Figures 7 through 11, the threshold behavior observed in load-reduction schemes [15-17] is caused by a rise in the crack-opening stresses, and the rise is caused by residual plastic deformations left in the wake of the growing crack. Thus, load-reduction schemes create artifically high values of stress-intensity factor thresholds, and the crack-growth rate data generated under these load-reduction schemes cannot be used in an LEFM analysis to predict the growth of small cracks. To obtain crack-growth rate data at low ΔK levels using large cracks, the threshold testing procedures must be changed. The residual deformations on the crack surfaces near the beginning of a threshold test must be eliminated (see insert in Fig. 8). The deformations could be machined away during the test or large compressive loads could be applied to the specimen to remove this deformation. The specimen could also have been side-grooved to eliminate plane-stress conditions at the crack front.

Growth of Small Cracks

In the following sections, the crack-growth rates measured in specimens with large cracks (c_o > 2 mm) are correlated with the plastic-zone corrected stress-intensity factor range, $\Delta\bar{K}_{eff}$. This correlation, a table of $\Delta\bar{K}_{eff}$ against dc/dN, provides the crack-growth rate data for the particular material and thickness. Using the closure model with an assumed constraint factor, the crack-growth rates for small cracks in plates and from holes are predicted and compared with experimental rates. All initial cracks are assumed to have no previous load history (no residual deformations).

6-8 CSA G40.11 Steel.- El Haddad [3] tested CCT and single-edge-crack tension (SECT) specimens made of the CSA G40.11 steel under cyclic loading at an R ratio of -1. The material yield stress was 370 MPa and the ultimate tensile strength was 510 MPa. All specimens were 2.54 mm thick. These tests were conducted to study the growth characteristics of small and large cracks.

The ΔK-rate data for the SECT specimens with large cracks are shown in Figure 12 as solid symbols. Because the closure model has not been developed for SECT specimens, the data were assumed to be equivalent to data generated on CCT specimens. (El Haddad's data on CCT specimens, to be shown later, were in good agreement with the SECT specimen data.) The solid lines through the SECT specimen data in Figure 12 show the baseline (ΔK-rate) data. To determine $\Delta\bar{K}_{eff}$, a closure analysis on a CCT specimen (S_{max} = 135 MPa; α = 1) was conducted. The corresponding crack-growth table is:

$\frac{dc}{dN}$, mm/cycle	$\Delta\bar{K}_{eff}$, MPa-$m^{1/2}$
2.24E-06	6.53
1.02E-05	7.69
4.70E-05	9.78
1.02E-04	12.62
1.93E-04	17.29
3.18E-04	22.46
6.60E-04	34.20
1.52E-03	58.31

This table was used in all predictions made on the CSA G40.11 steel.

El Haddad [3] tested CCT specimens with small cracks at high stress levels (207 and 240 MPa). The crack-starter notch was a very small hole (r = 0.19 mm), but no details were given on how the crack was initiated. These results are shown as the open symbols in Figure 12 and show that small cracks grow much faster than large cracks at the same ΔK level.

In the closure analysis, an extremely small through crack (0.01 mm) was assumed to exist at the edge of the starter notch. The constraint factor was assumed to be unity because the specimens were subjected to high stress levels. The predicted growth rates are shown as solid curves in Figure 12. The predictions are in fair agreement with the experimental results. Both experimental and predicted results show a minimum rate at a particular ΔK level. In the analysis, this behavior was caused by the transient behavior of the crack-opening stresses shown in Figure 13. Here the calculated S_o/S_{max} ratios are plotted against crack length for the two tests. The calculated crack-opening stress was initially the minimum applied stress, but the opening stress rapidly rose and then tended to level off as the crack grew under cyclic loading. Truyens [39] has experimentally shown a similar trend in S_o with crack length in a ship steel. The effective-stress range (ΔS_{eff}), indicated in the figure, was $S_{max} - S_o$. Crack-growth rates are directly related to ΔS_{eff}. As the crack grew, the decrease in ΔS_{eff} and the increase in crack length (increase in stress-intensity factor) combined to cause the unusual behavior shown in Figure 12. Truyens [39] also observed a similar trend in crack-growth rates.

El Haddad [3] also tested specimens with cracks emanating from larger holes than that used in the previous example. The hole radii were 4.76 and 7.94 mm in 70-mm-wide specimens. The maximum applied stress was 135 MPa at an R ratio of -1. His experimental data on the cracked-hole specimens are shown as open symbols in Figure 14. The solid symbols show his results from CCT specimens also tested at an applied stress level of 135 MPa. These results show that small cracks from holes grow much faster than would be predicted from using LEFM analyses with large crack data.

In the analysis, the baseline (ΔK-rate) data were obtained from large cracks in CCT and SECT specimens. The solid lines through the CCT specimen data in Figure 14 show the baseline data. Here again, no details on the crack-starter notch were given in Reference 3. Therefore, it was assumed that a very small through-crack (0.01 mm) was at the edge of the holes. The solid curves in Figure 14 show predictions from the closure analysis with α = 1. The predicted rates were in reasonable agreement with the experimental data. For cracks emanating from holes, the transient behavior of the crack-opening stresses (similar to that shown in Fig. 13) and the plastic-zone corrected stress-intensity factor range combined to cause the trends shown in Figure 14.

Alclad 2024-T3 Aluminum Alloy.- Broek [5] tested center-crack and cracked-hole specimens made of 2024-T3 Alclad aluminum alloy subjected to tensile loading at an R ratio of 0.01. The yield stress of the material was 375 MPa and the ultimate tensile strength was 475 MPa. All specimens were 2 mm thick. The ΔK-rate data are shown in Figure 15 for the CCT specimens and for specimens with small cracks emanating from holes of various radii, ranging from 2.5 to 20 mm. Again, these results show that small cracks from holes grow faster than would be predicted using an LEFM analysis with large crack data on CCT specimens.

6-9

In the closure analysis, the constraint factor was assumed to be unity because most of the rates were above the rate at transition (flat to slant growth). The rate at transition was estimated to be about 3×10^{-5} mm/cycle (first knee in baseline data at about 9 MPa-$m^{1/2}$). The development of the crack-growth rate table was discussed and was included in the section on "Fatigue Crack Growth Rates." The predicted results for small cracks at holes are shown as solid curves in Figure 15. Solid and open symbols of the same type denote corresponding predictions and experiments. For small radii, the analysis underpredicted the growth rates; for the larger radii, the analysis overpredicted the rates. In all cases, the predicted rates were within about a factor of 2 of the experimental rates.

Cast Nickel-Aluminum-Bronze Alloy.- Taylor and Knott [10,40] tested through-cracks and small surface cracks under three-point bending at an R ratio of 0.1. The material yield stress was 250 MPa. The ultimate tensile strength was not reported in References 10 or 40, and the strength was estimated to be 550 MPa [41]. Most of the surface-crack tests were conducted with a maximum outer fiber stress of 330 MPa [40]. The small surface cracks were naturally-occurring cracks from casting defects on the surface of the specimens. Some of the largest defects shown on photomicrographs [10,40] had lengths (2c) ranging from 0.05 to 0.15 mm. The ΔK-rate data for the surface-crack specimens are shown as open symbols in Figure 16. Reference 10 did not give the particular test conditions for each surface-crack test, but the test conditions were assumed to be identical. Thus, the data show a lot of scatter which is undoubtedly due to the cracks growing through different microstructure.

The solid curve showing the threshold at about 7.5 MPa-$m^{1/2}$ was obtained from bend specimens with large through-cracks. The results on large cracks and small surface cracks show that small cracks grow at ΔK levels well below the threshold established from large crack tests. (Again, the details of the large crack tests were not reported in References 10 or 40.)

Because crack-growth rate data generated under load-reduction schemes (see comments in section on "Threshold Testing") cannot be applied to the growth of small cracks [2], the dash-dot curve was assumed to be the baseline data. In the closure analysis, the constraint factor was assumed to be either 1 (plane stress) or 3 (plane strain). The crack-growth rate table for the corresponding constraint factors is:

$\frac{dc}{dN}$, mm/cycle	$\Delta\bar{K}_{eff}(\alpha = 1)$, MPa-$m^{1/2}$	$\Delta\bar{K}_{eff}(\alpha = 3)$, MPa-$m^{1/2}$
2.54E-09	1.62	2.55
2.77E-06	5.88	9.28
6.59E-06	6.84	10.78
1.31E-05	7.71	12.18
3.19E-05	9.23	14.58
7.59E-05	11.07	17.46

The closure analysis has only been developed for through-the-thickness crack configurations. To analyze the growth of a small surface crack under bending, the analysis for the CCT specimen was used with modification. In the analysis, the CCT specimen was subjected to an applied stress level equal to the outer fiber bending stress. For small surface cracks, this assumption is adequate [42]. The crack-depth-to-crack-length (a/c) ratios for the experiments were reported to be about 0.8 [10]. For this a/c ratio and for small surface cracks (a/t nearly zero), the average stress-intensity factor around the crack front is about

$$\Delta K = \Delta S \sqrt{\pi c}\, 0.7 \qquad (4)$$

Thus, the stress-intensity factor for the CCT specimen was multiplied by 0.7 to convert the equation to a small surface crack under bending. The crack-opening stresses calculated for a center-crack specimen were also assumed to apply for the surface-crack configuration.

The predicted results for small surface cracks are shown as solid curves in Figure 16 for the respective values of α. The plane-strain predictions were closer to the experimental results than the plane-stress predictions. However, under plane-strain conditions, the initial high growth rate (solid symbol) was considerably lower than the experimental rates. This discrepancy may be due to the crack growing in some "weak" direction in the microstructure in the early stages [10].

CONCLUSIONS

An analytical fatigue crack-closure model was used to study the crack growth and closure behavior of small cracks in plates and at circular holes, and to study the closure

6-10 behavior of large cracks under load-reduction schemes used in threshold testing. Some comparisons were made between calculated and experimental crack-opening stresses for these loading conditions on a steel and an aluminum alloy.

Crack-growth rates under constant-amplitude loading for large cracks (lengths greater than 2 mm) in a steel, an aluminum alloy, and a cast nickel-aluminum-bronze alloy were correlated with the plastic-zone corrected effective stress-intensity factor range. Using these correlations, the growth rates for small cracks in plates and at circular holes were predicted and compared with experimental growth rates.

The following conclusions were obtained:

1. Under load-reduction schemes used in threshold testing, the rise in crack-opening stresses near threshold is caused by residual plastic deformations. Thus, load-reduction schemes create artificially high values of stress-intensity factor thresholds.

2. Near threshold, the calculated crack-opening stresses under plane-stress conditions agreed well with experimental measurements on steel specimens.

3. Crack-growth rate data generated under load-reduction schemes for large cracks cannot be used with linear-elastic fracture mechanics analyses to accurately predict the growth of small cracks.

4. Small cracks (less than 1 mm) in plates and at holes grow faster than large cracks (greater than 2 mm) at equal stress-intensity factor ranges because the applied stress needed to open a small crack is less than that needed to open a large crack and, consequently, the effective stress range for small cracks is greater than that for large cracks.

5. Closure analyses based on plastic-zone corrected effective stress-intensity factor ranges and crack-growth rate data from large cracks predicted the growth of small cracks in plates and at holes reasonably well.

APPENDIX A--EQUATIONS FOR STRESS-INTENSITY FACTORS AND CRACK-SURFACE DISPLACEMENTS

The analytical closure model for a crack in a finite plate [25] and for cracks emanating from a circular hole in a finite plate requires the stress-intensity factor and crack-surface displacement equations for the two elastic configurations shown in Figure 17. The equations for stress-intensity factors and crack-surface displacements for a crack subjected to various loading in an infinite plate (r = 0) were obtained from the literature [43]. These equations are modified herein for cracks emanating from a circular hole in a finite plate. Some of the approximate equations are verified with boundary-collocation [44,45] and conformal-mapping [46,47] analyses.

Stress-Intensity Factors for Cracks Emanating from a Circular Hole in an Infinite Plate

Remote Uniform Stress.- The stress-intensity factor equation for the configuration shown in Figure 17(a), with w equal to infinity, was obtained by fitting to the results from References 45 and 47. The equation is

$$K_h^S = K_\infty^S F_h^S = S\sqrt{\pi d}\, F_h^S \tag{5}$$

where K_∞^S is for a crack in an infinite plate without a hole and F_h^S is the boundary-correction factor for the circular hole. The equation for F_h^S is

$$F_h^S = \sqrt{1 - \frac{r}{d}}\, f_n \tag{6}$$

where $n = 1$ is for a single crack and $n = 2$ is for two symmetric cracks. The functions f_n are

$$f_1 = 0.707 + 0.765\lambda + 0.282\lambda^2 + 0.74\lambda^3 + 0.872\lambda^4 \tag{7}$$

and

$$f_2 = 1 + 0.358\lambda + 1.425\lambda^2 - 1.578\lambda^3 + 2.156\lambda^4 \tag{8}$$

where $\lambda = r/d$ and $0 \le \lambda < 1$. Eq. (5) is within 0.2 percent of the results in References 45 and 47.

Concentrated Force.- The stress-intensity factors for two cracks emanating from a circular hole subjected to a symmetric pair of concentrated forces in an infinite plate,

Figure 18, were obtained from a boundary-collocation analysis by Newman (unpublished). An equation was fitted to the results and is

$$K_h^p = K_\infty^p F_h^p = \frac{2Pd}{\sqrt{\pi d\left(d^2 - b^2\right)}} F_h^p \tag{9}$$

where K_∞^p is for a crack in an infinite plate without a hole and F_h^p is the boundary-correction factor for the circular hole. The equation for the correction factor is

$$F_h^p = 1 + A_1\left(\frac{1 - \gamma}{1 - \lambda}\right) + A_2\left(\frac{1 - \gamma}{1 - \lambda}\right)^2 \tag{10}$$

$$A_1 = -0.02\lambda^2 + 0.558\lambda^4 \tag{11}$$

$$A_2 = 0.221\lambda^2 + 0.046\lambda^4 \tag{12}$$

where $\gamma = b/d$ and $\lambda = r/d$ for $\lambda \le \gamma \le 1$ and $0 \le \lambda < 1$. Eq. (9) is within ±1 percent of the boundary-collocation results.

Partially-Loaded Crack.- The stress-intensity factors for the configuration and loading shown in Figure 17(b), with $w = \infty$, were obtained by using Eq. (9) as a Green's function and integrating over the segment b_1 to b_2. The resulting equation is

$$K_h^\sigma = \frac{2\sigma}{\pi}\sqrt{\pi d}\, G(\gamma,\lambda) \tag{13}$$

where

$$G(\gamma,\lambda) = \left\{\left[1 + \frac{A_1}{1 - \lambda} + \frac{3A_2}{2(1 - \lambda)^2}\right]\sin^{-1}\gamma + \left[\frac{A_1}{1 - \lambda} + \frac{(4 - \gamma)A_2}{2(1 - \lambda)^2}\right]\sqrt{1 - \gamma^2}\right\}\Bigg|_{\gamma = b_1/d}^{\gamma = b_2/d} \tag{14}$$

A_1 and A_2 are given by Eqs. (11) and (12), respectively. To get Eq. (13) into the same form as Eqs. (5) and (9), Eq. (13) is rewritten as

$$K_h^\sigma = K_\infty^\sigma F_h = \frac{2\sigma}{\pi}\sqrt{\pi d}\left[\sin^{-1}\left(\frac{b_2}{d}\right) - \sin^{-1}\left(\frac{b_1}{d}\right)\right] F_h^\sigma \tag{15}$$

where K_∞^σ is for a crack in an infinite plate without a hole and F_h^σ is the circular hole correction factor. The function F_h^σ is given by

$$F_h^\sigma = \frac{G(\gamma,\lambda)}{\sin^{-1}\left(\frac{b_2}{d}\right) - \sin^{-1}\left(\frac{b_1}{d}\right)} \tag{16}$$

where $G(\gamma,\lambda)$ is given by Eq. (14).

Crack-Surface Displacements for Cracks Emanating from a Circular Hole in an Infinite Plate

The exact crack-surface displacements for the configurations shown in Figure 17, with w equal to infinity and hole radius equal to zero, were obtained from Westergaard stress functions given in Reference 43. These equations are modified herein for cracks emanating from a circular hole. The following sections given approximate displacement equations for remote uniform stress and for the partially-loaded crack.

Remote Uniform Stress.- The approximate crack-surface displacements for the configurations shown in Figure 17(a), with $w = \infty$, are

$$V_h^s = \frac{2(1 - n^2)S}{E}\sqrt{d^2 - x^2}\, F_h^s \tag{17}$$

for $|x| \le d$, where $n = \nu$ for plane strain and $n = 0$ for plane stress. F_h^s is given by Eq. (6). In the region near the crack tip, Eq. (17) is very accurate.

6-12 Partially-Loaded Crack.- The approximate crack-surface displacements for the configuration and loading shown in Figure 17(b), with $w = \infty$, are

$$V_h^\sigma = [V_\infty(x) + V_\infty(-x)]F_h^\sigma \tag{18}$$

where

$$V_\infty(x) = \frac{2(1-\nu^2)\sigma}{\pi E}\left[(b-x)\cosh^{-1}\left(\frac{d^2-bx}{d|b-x|}\right) + \sqrt{d^2-x^2}\sin^{-1}\left(\frac{b}{d}\right)\right]\Bigg|_{b=b_1}^{b=b_2} \tag{19}$$

for $|x| \le d$, and F_h^σ is given by Eq. (16). Again, the equation is very accurate in the region near the crack tip.

Finite-Width Corrections

The equations given in the preceding sections for stress-intensity factors and crack-surface displacements (Eqs. (5) to (19)) are for cracks emanating from a circular hole in an infinite plate. But these quantities are influenced by the finite width of the plate. Therefore, some approximate finite-width corrections are developed herein. The stress-intensity factor for a crack in a finite-width plate is

$$K = K_\infty F_w \tag{20}$$

where K_∞ is the stress-intensity factor for cracks emanating from a circular hole in an infinite plate and F_w is the finite-width correction for the particular loading condition. Noting that the elastic crack-surface displacements in the region of the crack tip are directly related to the stress-intensity factor, it is proposed that the same correction factor be used for displacements:

$$V = V_\infty\left(\frac{K}{K_\infty}\right) = V_\infty F_w \tag{21}$$

where V_∞ is the displacement for cracks emanating from a circular hole in an infinite plate, again subjected to the particular loading condition. Eq. (21) gives very accurate crack-surface displacements in the region near the crack tip.

Remote Uniform Stress.- The approximate boundary-correction factor for two symmetric cracks emanating from a circular hole in a finite-width plate subjected to uniform stress [48], as shown in Figure 17(a), is

$$F_w^S = \sqrt{\sec\left(\frac{\pi r}{2w}\right)\sec\left(\frac{\pi d}{2w}\right)} \tag{22}$$

for $r/w \le 0.5$ and $d/w \le 0.7$. Eq. (22) is within 2 percent of boundary-collocation results [45]. The equation accounts for the influence of width on stress concentrations at the edge of the hole [49] and the influence of width on stress-intensity factors. The crack-surface displacements given by Eqs. (17), (21), and (22) for $r = 0$ were compared with results from Reference 44, which used the boundary-collocation method. The displacements were within 2 percent of each other for any value of x for $d/w \le 0.7$. The displacements near the crack tip were very accurate, as expected.

Partially-Loaded Crack.- The approximate boundary-correction factor for two symmetric cracks emanating from a circular hole in a finite-width plate subjected to partial loading on the crack surface (Fig. 17(b)) was obtained from the infinite periodic array of cracks ($r = 0$) solution [43]. The correction factor is modified herein, as was done in Reference 25, and is given by

$$F_w^\sigma = \left[\frac{\sin^{-1}B_2 - \sin^{-1}B_1}{\sin^{-1}\left(\frac{b_2}{d}\right) - \sin^{-1}\left(\frac{b_1}{d}\right)}\right]\sqrt{\sec\left(\frac{\pi d}{2w}\right)} \tag{23}$$

where

$$B_k = \sin\left(\pi b_k/2w\right)/\sin\left(\pi d/2w\right) \tag{24}$$

for $r/w \le 0.25$ and $d/w \le 0.7$.

APPENDIX B--CALCULATION OF CRACK-OPENING STRESS

The following section describes the method used to calculate the crack-opening stresses in the analytical closure model. To find the applied stress level needed to open the crack surface at any point, the displacement at that point due to an applied stress increment $(S_o - S_{min})$ is set equal to the displacement at that point due to the contact stresses at S_{min}. This calculation is made at the centroid of all elements in contact along the crack surface. The maximum value of $(S_o - S_{min})$ gives the applied stress level at which the last element (in contact) separates (or opens). This approach is possible because the stresses on the elements are elastic until the crack-tip element yields. Crack-tip element yielding occurs only after the crack surfaces open (see Figs. 4 and 8).

The displacement at point i, along the crack surface, due to an applied stress increment is

$$V_i^s = (S_o - S_{min}) f(x_i) \tag{25}$$

where

$$f(x_i) = \frac{2(1 - \eta^2)}{E} \sqrt{c^2 - x_i^2}\, F_h^s F_w^s \tag{26}$$

F_h^s and F_w^s are given by Eqs. (6) and (22), respectively, with d replaced by c. The displacement at point i due to contact stresses is

$$V_i^\sigma = \sum_{j=11}^{n} \sigma_j g(x_i, x_j) \tag{27}$$

where

$$g(x_i, x_j) = G(x_i, x_j) + G(-x_i, x_j) \tag{28}$$

$$G(x_i, x_j) = \frac{2(1 - \eta^2)}{\pi E} \left\{ (b_2 - x_i) \cosh^{-1}\left(\frac{c^2 - b_2 x_i}{c|b_2 - x_i|}\right) - (b_1 - x_i) \cosh^{-1}\left(\frac{c^2 - b_1 x_i}{c|b_1 - x_i|}\right) + \sqrt{c^2 - x_i^2}\left[\sin^{-1}\left(\frac{b_2}{c}\right) - \sin^{-1}\left(\frac{b_1}{c}\right)\right] \right\} F_h^\sigma F_w^\sigma \tag{29}$$

$b_1 = x_j - w_j$ and $b_2 = x_j + w_j$ (w_j is the half width of bar element at point j). (In the closure model, 10 elements were used in the plastic zone and elements 11 to n were residual plastic deformation elements along the crack surface (see Ref. 25 for details).) F_h^σ and F_w^σ are given by Eqs. (16) and (23), respectively, again with d replaced by c. Equating Eqs. (25) and (27), and solving for $(S_o)_i$, gives

$$(S_o)_i = S_{min} + \sum_{j=11}^{n} \sigma_j g(x_i, x_j) \Big/ f(x_i) \tag{30}$$

for i = 11 to n. The maximum value of $(S_o)_i$ gives the crack-opening stress, S_o.

APPENDIX C--CALCULATION OF PLASTIC-ZONE SIZE

Center-Crack Tension Specimen

The plastic-zone size (ρ) for a crack in a finite-width specimen (Fig. 2(a)) was obtained from Rice [50] and rederived by Newman [25] as

$$\rho = c\left\{\left(\frac{2w}{\pi c}\right)\sin^{-1}\left[\sin\left(\frac{\pi c}{2w}\right)\sec\left(\frac{\pi S_{max}}{2\alpha\sigma_o}\right)\right] - 1\right\} \tag{31}$$

For $\alpha = 1$, the equation reduces to the expression derived by Rice from an infinite periodic array of cracks solution. Newman derived the equation from approximate stress-intensity factor equations for finite-width specimens.

Cracked-Hole Specimen

The plastic-zone size for cracks emanating from a circular hole in a finite-width specimen (Fig. 2(b)) was determined by requiring that the finiteness condition of Dugdale [26] be satisfied. This condition states that the stress-intensity factor at the tip of the plastic zone is zero and is given by

$$K_h^S + K_h^\sigma = 0 \tag{32}$$

where

$$K_h^S = S_{max}\sqrt{\pi d}\, F_h^S F_w^S \tag{33}$$

and

$$K_h^\sigma = -\frac{2\alpha\sigma_o}{\pi}\sqrt{\pi d}\left[\frac{\pi}{2} - \sin^{-1}\left(\frac{c}{d}\right)\right] F_h^\sigma F_w^\sigma \tag{34}$$

F_h^S and F_w^S are given by Eqs. (6) and (22), respectively. F_h^σ and F_w^σ were obtained from Eqs. (16) and (23), respectively, by setting $b_1 = c$ and $b_2 = d$. Substituting Eqs. (33) and (34) into Eq. (32) and simplifying gives

$$S_{max} F_h^S F_w^S - \alpha\sigma_o\left[1 - \frac{2}{\pi}\sin^{-1}\left(\frac{c}{d}\right)\right] F_h^\sigma F_w^\sigma = 0 \tag{35}$$

For a given applied stress S_{max}, constraint factor α, flow stress σ_o, specimen width w, hole radius r, and crack length c, Eq. (35) was solved for d by using an iterative technique. Noting that ρ is equal to $d - c$ gives the plastic-zone size.

The plastic-zone sizes for cracks emanating from a circular hole in an infinite plate subjected to remote uniform stress are shown in Figure 19. The plastic-zone size normalized by c is plotted against $S/(\alpha\sigma_o)$. The dashed curve ($r = 0$) shows the Dugdale model [26]. The solid curves show the normalized plastic-zone sizes for various c/r ratios. For c/r equal to unity, yielding does not occur for $S/(\alpha\sigma_o)$ ratios less than one-third or $1/K_T$, where K_T is the stress concentration for the circular hole.

REFERENCES

1. Pearson, S.: Initiation of Fatigue Cracks in Commercial Aluminum Alloys and the Subsequent Propagation of Very Short Cracks. Engineering Fracture Mechanics, Vol. 7, No. 2, 1975, pp. 235-247.

2. Kitagawa, H.; and Takahashi, S.: Applicability of Fracture Mechanics to Very Small Cracks or the Cracks in the Early Stage. Proceedings of the 2nd International Conference on Mechanical Behavior of Materials, Boston, MA, 1976, pp. 627-631.

3. El Haddad, M. H.: A Study of the Growth of Short Fatigue Cracks Based on Fracture Mechanics. Ph.D. Thesis, University of Waterloo, Waterloo, Ontario, Canada, 1978.

4. El Haddad, M. H.; Dowling, N. E.; Topper, T. H.; and Smith, K. N.: J Integral Applications for Short Fatigue Cracks at Notches. International Journal of Fracture, Vol. 16, No. 1, 1980, pp. 15-30.

5. Broek, D.: The Propagation of Fatigue Cracks Emanating from Holes. National Aerospace Laboratory, NLR Technical Report 72134U, 1972.

6. Morris, W. L.; James, M. R.; and Buck, O.: Growth Rate Models for Short Surface Cracks in Al 2219-T851. Metallurgical Trans. A, Vol. 12A, January 1981, pp. 57-64.

7. Hudak, S. J., Jr.: Small Crack Behavior and the Prediction of Fatigue Life. Journal of Engineering Materials and Technology, Vol. 103, 1981, pp. 26-35.

8. Nisitani, H.; and Takao, K. I.: Significance of Initiation, Propagation, and Closure of Microcracks in High Cycle Fatigue of Ductile Materials. Engineering Fracture Mechanics, Vol. 15, No. 3-4, 1981, pp. 445-456.

9. Schijve, J.: Difference Between the Growth of Small and Large Fatigue Cracks--The Relation to Threshold K-Values. Proceedings of the International Symposium on Fatigue Thresholds, Stockholm, Sweden, June 1981. (Also: Delft University of Technology Report LR-327, 1981.)

10. Taylor, D.; and Knott, J. F.: Fatigue Crack Propagation Behavior of Short Cracks--The Effects of Microstructure. Fatigue of Engineering Materials and Structures, Vol. 4, No. 2, 1981, pp. 147-155.

11. Leis, B. N.; and Forte, T. P.: Fatigue Growth of Initially Physically Short Cracks in Notched Aluminum and Steel Plates. Fracture Mechanics: Thirteenth Conference, Richard Roberts, ed., American Society for Testing and Materials, ASTM STP 743, 1981, pp. 100-124.

12. Elber, W.: Fatigue Crack Closure Under Cyclic Tension. Engineering Fracture Mechanics, Vol. 2, No. 1, 1970, pp. 37-45.

13. Elber, W.: The Significance of Fatigue Crack Closure. Damage Tolerance in Aircraft Structures, American Society for Testing and Materials, ASTM STP 486, 1971, pp. 230-242.

14. Paris, P. C.: Testing for Very Slow Growth of Fatigue Cracks. Closed Loop Magazine, MTS Systems Corporation, Vol. 2, No. 5, 1970.

15. Ohta, A.; and Sasaki, E.: A Method for Determining the Stress Intensity Threshold Level for Fatigue Crack Propagation. Engineering Fracture Mechanics, Vol. 9, No. 3, 1977, pp. 655-662.

16. Robin, C.; and Pluvinage, G.: Fatigue Threshold in a 2618A Aluminum Alloy. Fatigue of Engineering Materials and Structures, Vol. 3, 1980, pp. 147-157.

17. Bucci, R. J.: Development of a Proposed ASTM Standard Test Method for Near-Threshold Fatigue Crack Growth Rate Measurement. Fatigue Crack Growth Measurement and Data Analysis, S. J. Hudak, Jr., and R. J. Bucci, eds., American Society for Testing and Materials, ASTM STP 738, 1981, pp. 5-28.

18. Frandsen, J. D.; Inman, R. V.; and Buck, O.: A Comparison of Acoustic and Strain Gauge Techniques for Crack Closure. International Journal of Fracture, Vol. 11, No. 2, 1975, pp. 345-348.

19. Ohta, A.; Kosuge, M.; and Sasaki, E.: Fatigue Crack Closure Over the Range of Stress Ratios from -1 to 0.8 Down to Stress Intensity Factor Threshold Level in HT80 Steel and SUS 304 Stainless Steel. International Journal of Fracture, Vol. 14, No. 3, 1978, pp. 251-264.

20. Minakawa, K.; and McEvily, A. J.: On Crack Closure in the Near-Threshold Region. Scripta Metallurgica, Vol. 15, 1981, pp. 633-636.

21. Ritchie, R. O.: Effects of Strength and Grain Size on Near-Threshold Fatigue Crack Growth in Ultra-High Strength Steel. Proceedings of the Fourth International Conference on Fracture, Waterloo, Ontario, Canada, 1977, pp. 1325-1331.

22. Nordmark, G. E.; and Fricke, W. G.: Fatigue Crack Arrest at Low Stress Intensities in a Corrosive Environment. Journal of Testing and Evaluation, Vol. 6, No. 5, 1978, pp. 301-303.

23. Newman, J. C., Jr.: Finite-Element Analysis of Fatigue Crack Propagation--Including the Effects of Crack Closure. Ph.D. Thesis, Virginia Polytechnic Institute and State University, Blacksburg, VA, May 1974.

24. Hardrath, H. F.; Newman, J. C., Jr.; Elber, W.; and Poe, C. C., Jr.: Recent Developments in Analysis of Crack Propagation and Fracture of Practical Materials. Fracture Mechanics, N. Perrone, ed., University Press of Virginia, 1978, pp. 347-364.

25. Newman, J. C., Jr.: A Crack-Closure Model for Predicting Fatigue Crack Growth Under Aircraft Spectrum Loading. Methods and Models for Predicting Fatigue Crack Growth Under Random Loading, J. B. Chang and C. M. Hudson, eds., American Society for Testing and Materials, ASTM STP 748, 1981, pp. 53-84.

26. Dugdale, D. S.: Yielding of Steel Sheets Containing Slits. Journal of Mechanics, Physics, and Solids, Vol. 8, No. 2, 1960, pp. 100-104.

27. Newman, J. C., Jr.: Fracture of Cracked Plates Under Plane Stress. Engineering Fracture Mechanics, Vol. 1, No. 1, 1968, pp. 137-154.

28. Irwin, G. R.: Plastic Zone Near a Crack and Fracture Toughness. Proceedings of the 7th Sagamore Conference, 1960, p. IV-63.

29. Newman, J. C., Jr.: Discussion on Cyclic Crack Growth Transitional Behavior. Fatigue Crack Propagation, American Society for Testing and Materials, ASTM STP 415, 1967, pp. 380-383.

30. Barenblatt, G. I.: Mathematical Theory of Equilibrium Cracks in Brittle Fracture. Advances in Applied Mechanics, Vol. 7, 1962.

31. Minakawa, K.; and McEvily, A. J.: On Near-Threshold Fatigue Crack Growth in Steels and Aluminum Alloys. Proceedings of the International Conference on Fatigue Thresholds, Vol. 2, Stockholm, Sweden, 1981, p. 36.

32. Walker, N.; and Beevers, C. J.: A Fatigue Crack Closure Mechanism in Titanium. Fatigue of Engineering Materials and Structures, Vol. 1, No. 1, 1979, pp. 135-148.

33. Paris, P. C.; Bucci, R. J.; Wessel, E. T.; Clark, W. G.; and Mager, T. R.: Extensive Study of Low Fatigue Crack Growth Rates in A533 and A508 Steels. Stress Analysis and Growth of Cracks, American Society for Testing and Materials, ASTM STP 513, 1972, pp. 141-176.

34. Ritchie, R. O.; Suresh, S.; and Moss, C. M.: Near-Threshold Fatigue Crack Growth in 2.25Cr-1Mo Pressure Vessel Steel in Air and Hydrogen. Journal of Engineering Materials and Technology, Vol. 102, 1980, pp. 293-299.

35. Ohtsuka, A.; Mori, K.; and Miyata, T.: The Condition of Fatigue Crack Growth in Mixed Mode Condition. Engineering Fracture Mechanics, Vol. 7, No. 3, 1975, pp. 429-439.

36. Ewalds, H. L.; and Furnee, R. T.: Crack Closure Measurement Along the Fatigue Crack Front of Center Cracked Specimens. International Journal of Fracture, Vol. 14, No. 2, 1978, pp. R53-R55.

37. Newman, J. C., Jr.: Prediction of Fatigue Crack Growth Under Variable-Amplitude Loading Using a Closure Model. Design of Fatigue and Fracture Resistant Structures, P. R. Abelkis and C. M. Hudson, eds., American Society for Testing and Materials, ASTM STP 761, 1982, pp. 255-277.

38. McEvily, A. J.: Current Aspects of Fatigue. Metal Science, August/September 1977, p. 284.

39. Truyens, P.: Crack Growth Under Variable Loads in Ships. Ph.D. Thesis, University of Gent, Gent, Belgium, 1976.

40. Taylor, D.; and Knott, J. F.: Growth of Fatigue Cracks from Casting Defects in Nickel Aluminum Bronze. Proceedings of the Metal Society Conference on Defects and Crack Initiation in Environment Sensitive Fracture, University of Newcastle-on-Tyne, 1981.

41. Metals Handbook, Properties and Selection of Metals. Vol. 1, 8th Ed., American Society for Metals, 1961.

42. Newman, J. C., Jr.; and Raju, I. S.: An Empirical Stress-Intensity Factor Equation for the Surface Crack. Engineering Fracture Mechanics, Vol. 15, No. 1-2, 1981, pp. 185-192.

43. Tada, H.; Paris, P. C.; and Irwin, G. R.: The Stress Analysis of Cracks Handbook. Del Research Corporation, 1973.

44. Newman, J. C., Jr.: Crack-Opening Displacements in Center-Crack, Compact, and Crack-Line Wedge-Loaded Specimens. NASA Technical Note D-8268, 1976.

45. Newman, J. C., Jr.: An Improved Method of Collocation for the Stress Analysis of Cracked Plates with Various Shaped Boundaries. NASA Technical Note D-6376, 1971.

46. Bowie, O. L.: Analysis of an Infinite Plate Containing Radial Cracks Originating at the Boundary of an Internal Circular Hole. Journal of Mathematics and Physics, Vol. XXXV, No. 1, 1956, pp. 60-71.

47. Shivakumar, V.; and Forman, R. G.: Green's Function for a Crack Emanating from a Circular Hole in an Infinite Sheet. International Journal of Fracture, Vol. 16, No. 4, 1980, pp. 305-316.

48. Newman, J. C., Jr.: Predicting Failure of Specimens with Either Surface Cracks or Corner Cracks at Holes. NASA Technical Note D-8244, 1976.

49. Howland, R. C. J.: On the Stresses in the Neighbourhood of a Circular Hole in a Strip Under Tension. Philosophical Transactions of the Royal Society of London, Series A, Vol. 229, 1930, pp. 49-86.

50. Rice, J. R.: The Mechanics of Crack Tip Deformations and Extension by Fatigue. Brown University Technical Report NSF GK-28613, May 1966.

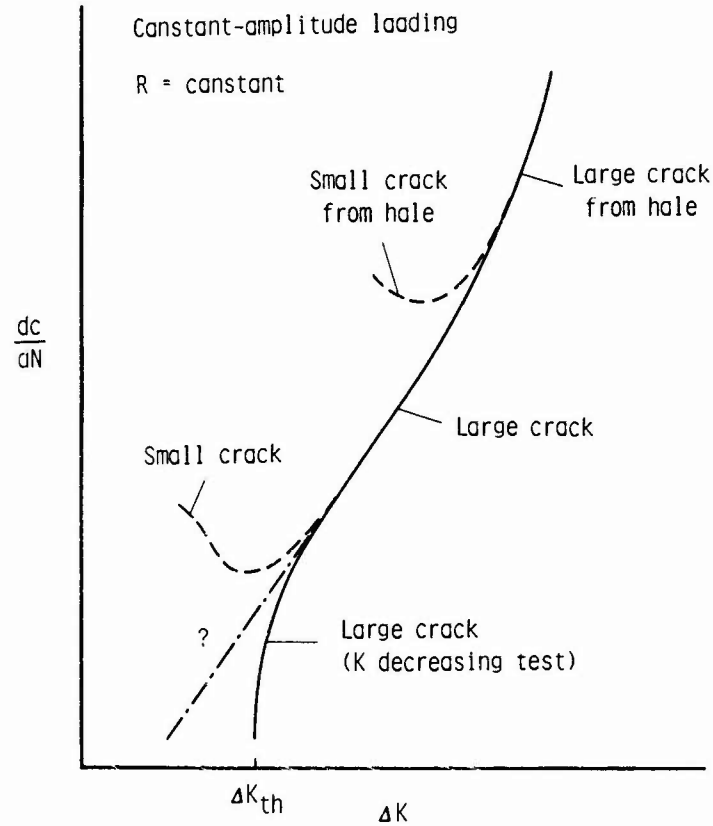

Figure 1.- Typical fatigue-crack growth rate data for small and large cracks.

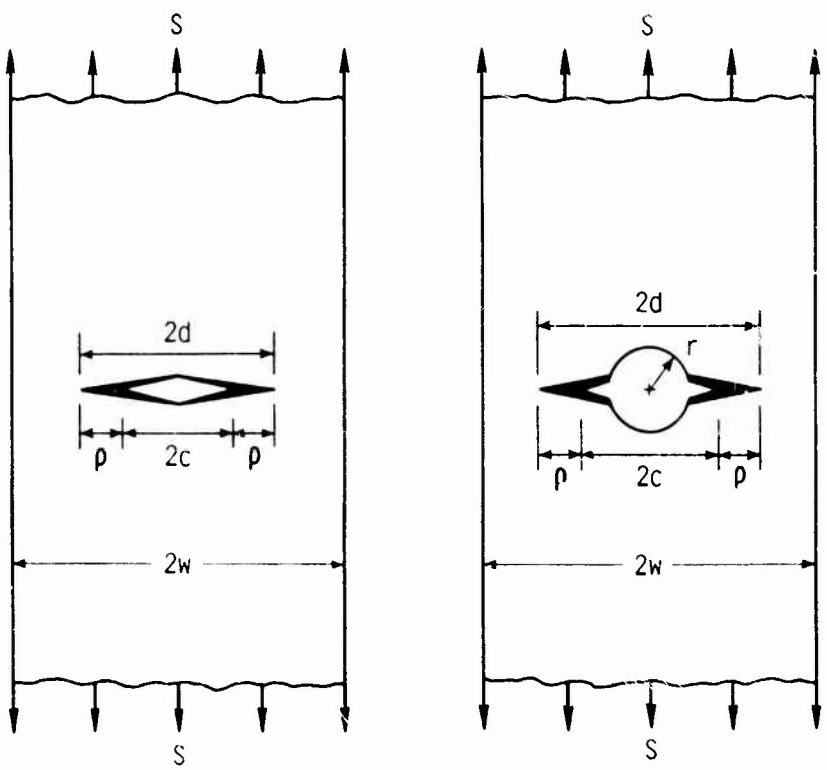

Figure 2.- Center-crack and cracks from circular hole specimens with Dugdale plastic zones and residual plastic deformations.

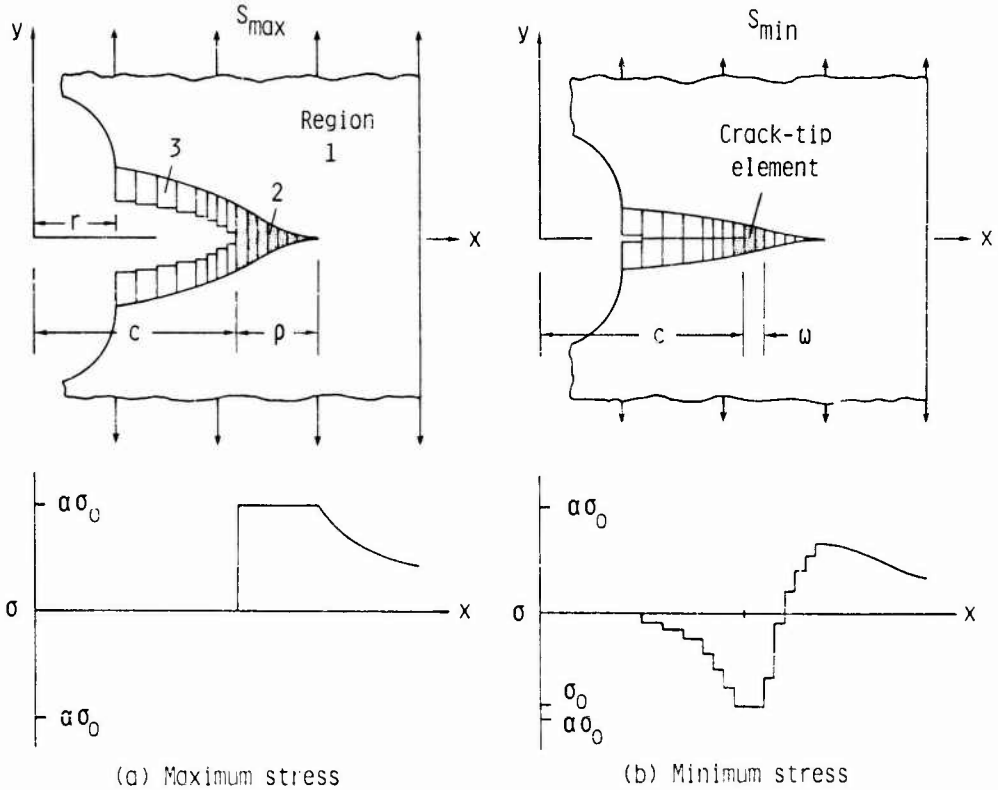

Figure 3.- Crack-surface displacements and stress distributions along crack line.

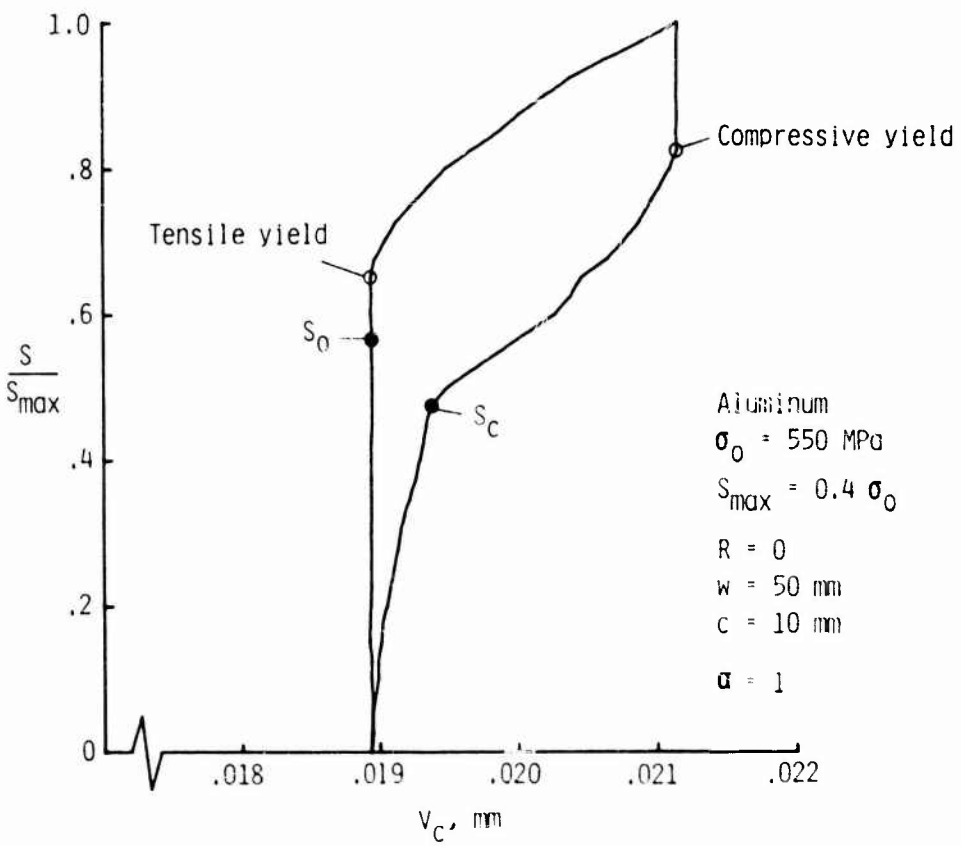

Figure 4.- Calculated displacement of crack-tip element under constant-amplitude loading.

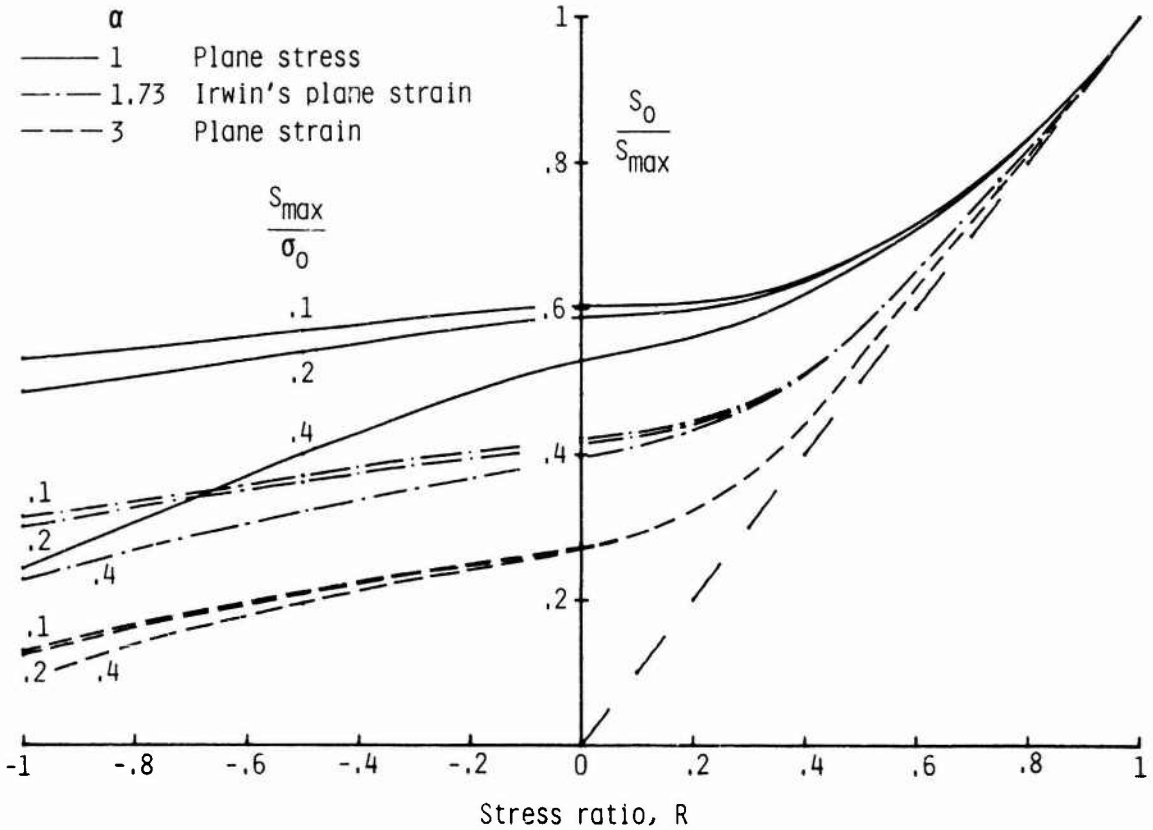

Figure 5.- Normalized crack-opening stresses as a function of R ratio under constant-amplitude loading for simulated plane-stress and plane-strain conditions.

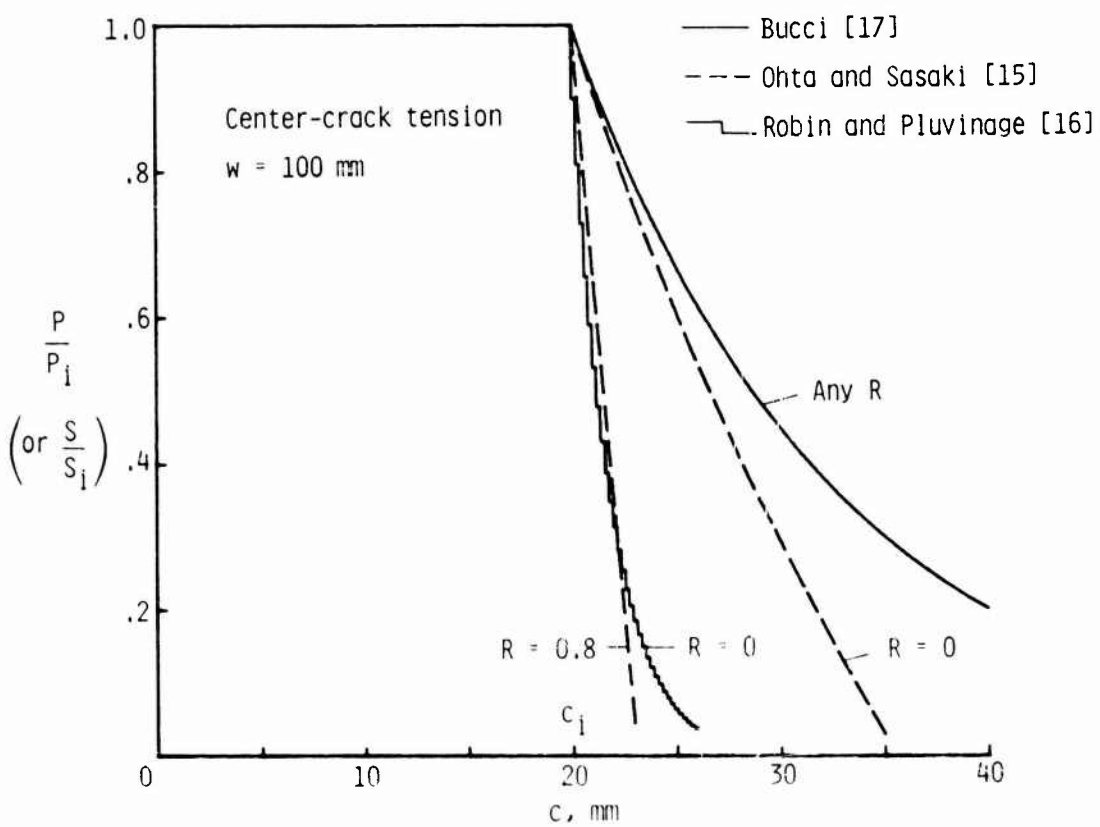

Figure 6.- Various load-reduction schemes used in ΔK threshold testing.

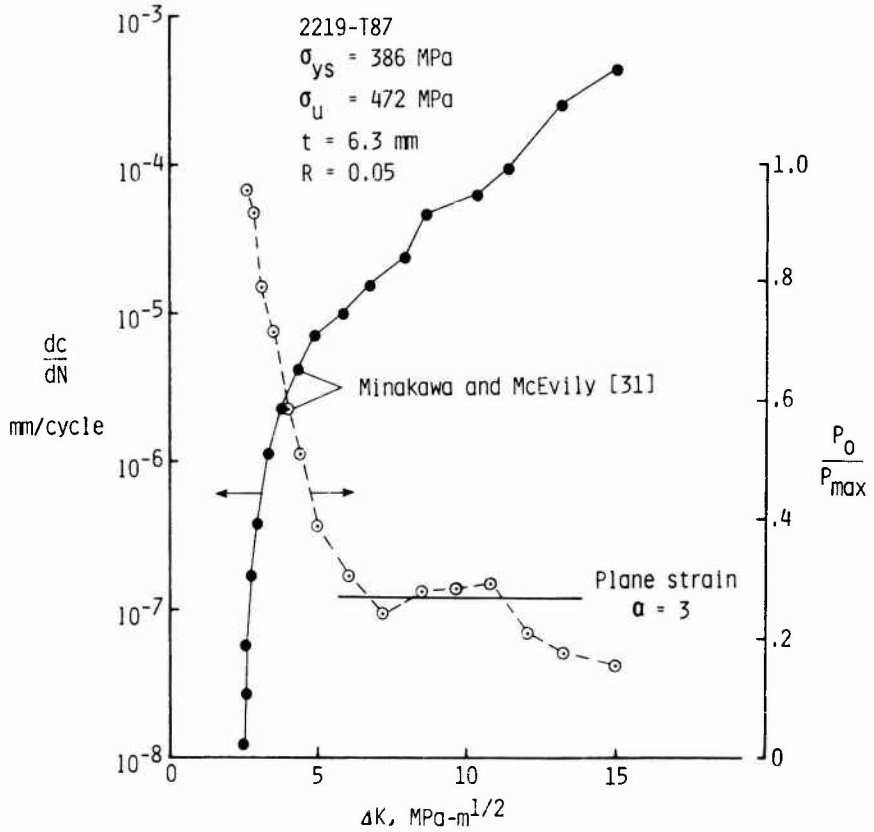

Figure 7.- Comparison of experimental growth rates and crack-opening stresses on a 2219-T87 aluminum alloy compact specimen [31].

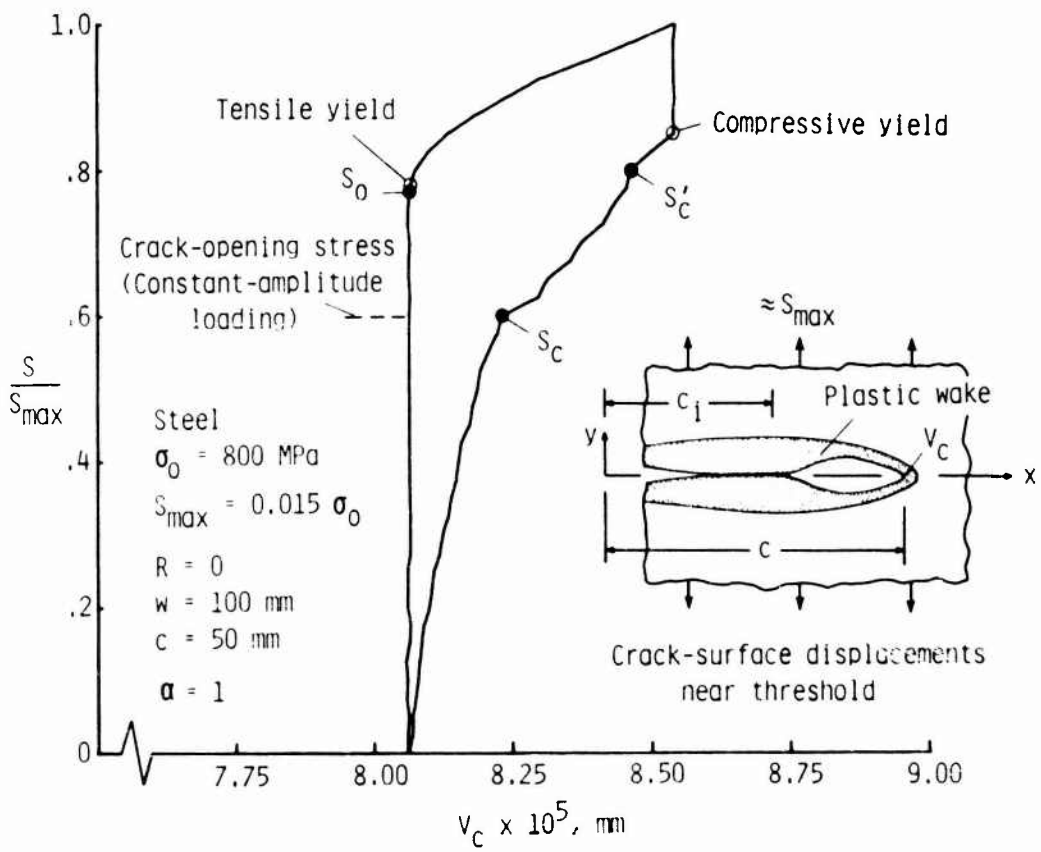

Figure 8.- Calculated displacement of crack-tip element for a ΔK-threshold test using Bucci's load-reduction scheme [17].

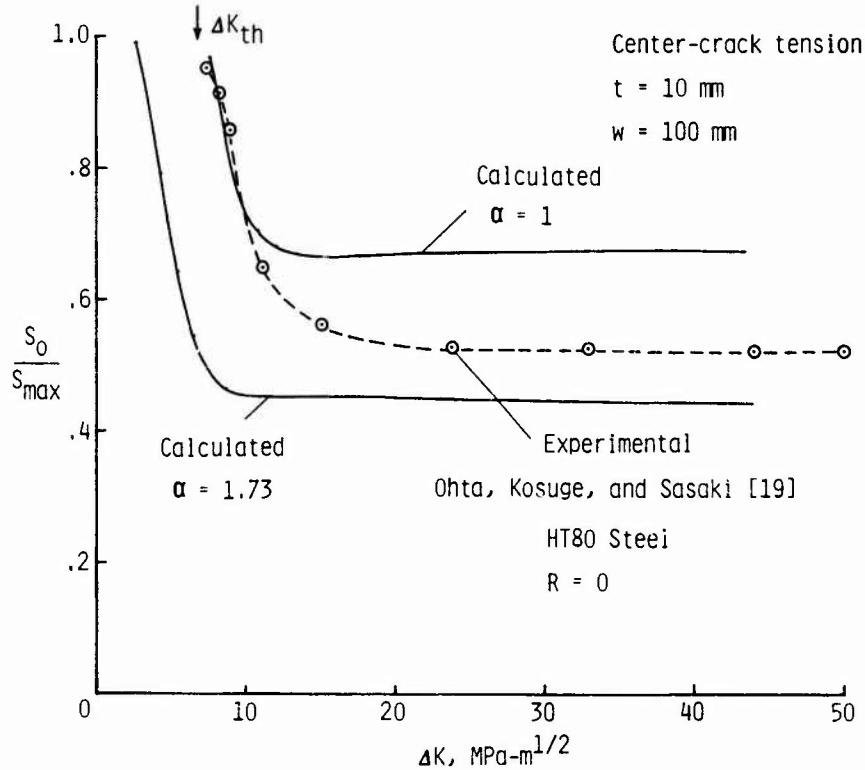

Figure 9.- Comparison of experimental and calculated crack-opening stresses for a ΔK-threshold test using Ohta-Sasaki load-reduction scheme [15].

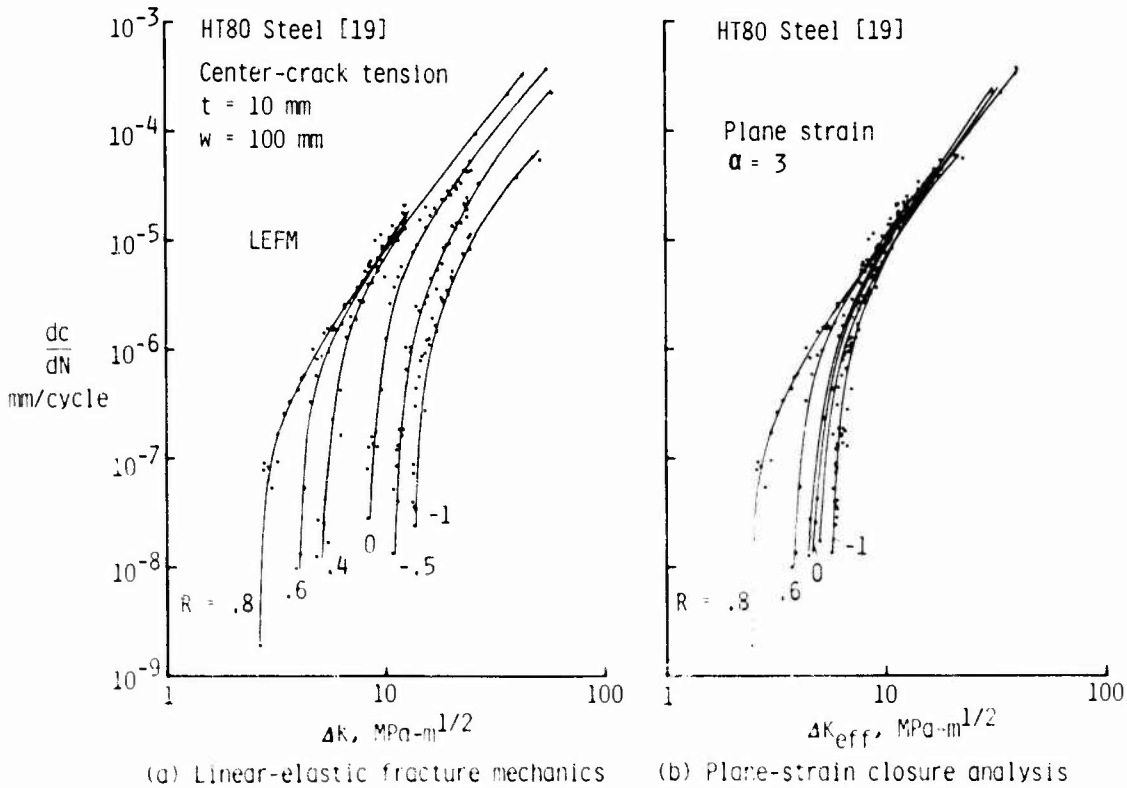

(a) Linear-elastic fracture mechanics (b) Plane-strain closure analysis

Figure 10.- Crack-growth rates as a function of stress-intensity factor range for various R ratios using LEFM and closure analysis for simulated plane-strain condition.

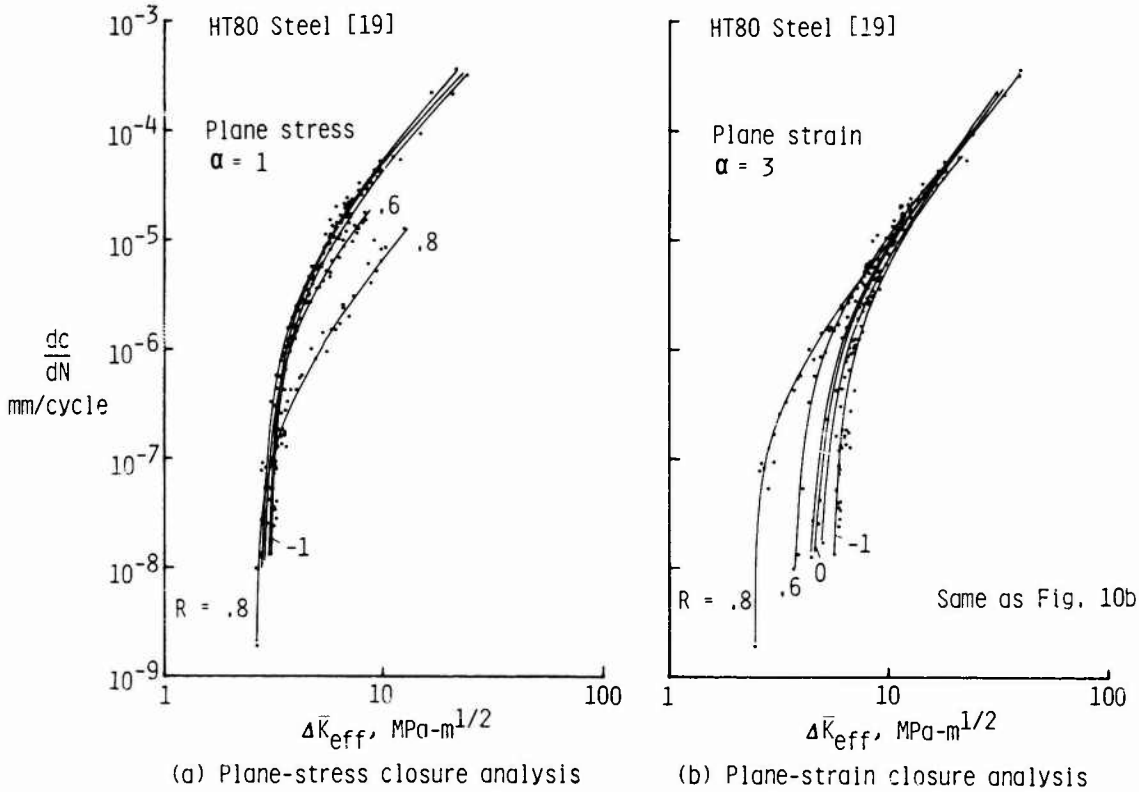

(a) Plane-stress closure analysis (b) Plane-strain closure analysis

Figure 11.- Crack-growth rates as a function of stress-intensity factor range for various R ratios using closure analyses for simulated plane-stress and plane-strain conditions.

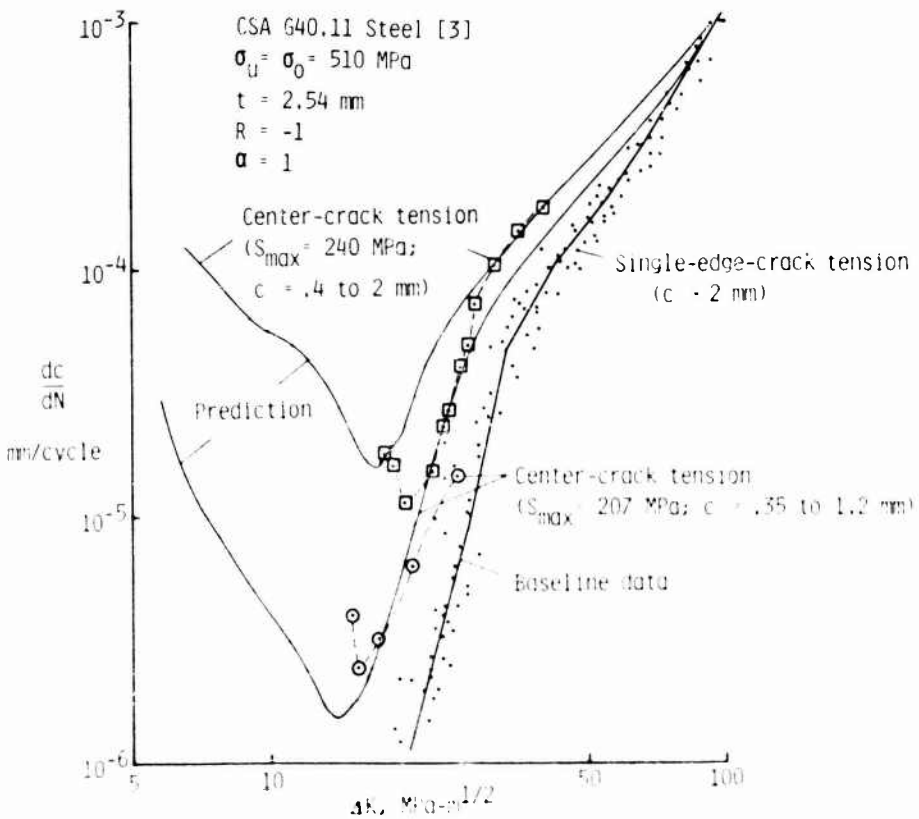

Figure 12.- Comparison of experimental and predicted crack-growth rates for small cracks in center-crack tension specimens subjected to high stress levels.

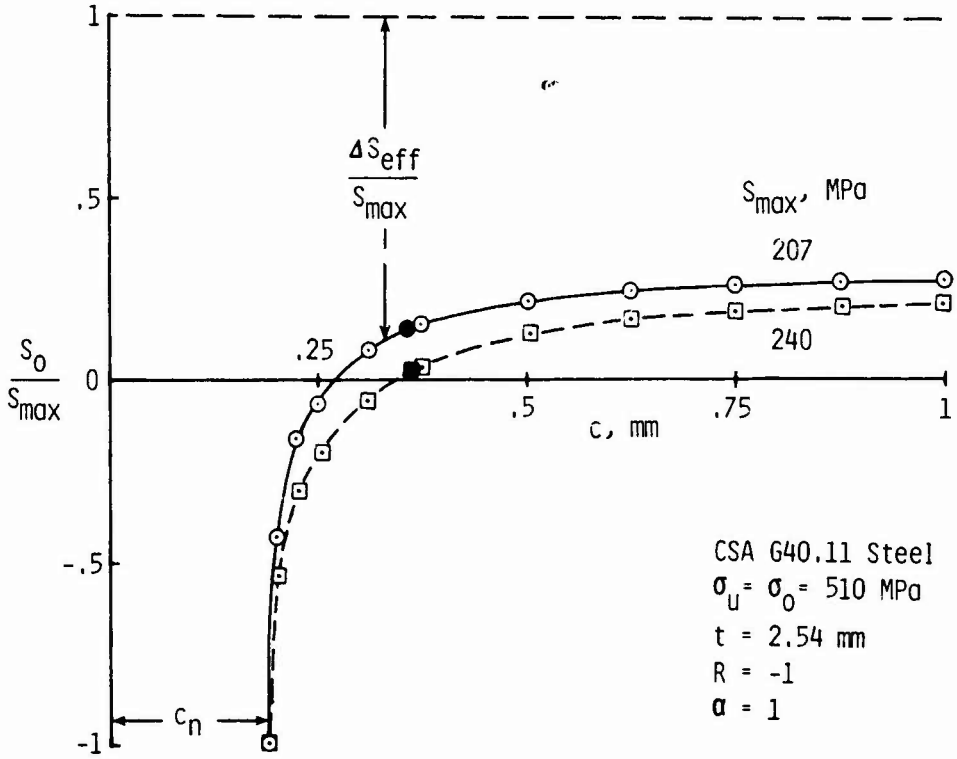

Figure 13.- Calculated crack-opening stresses as a function of crack length under constant-amplitude loading (solid symbol denotes crack length at minimum crack-growth rate).

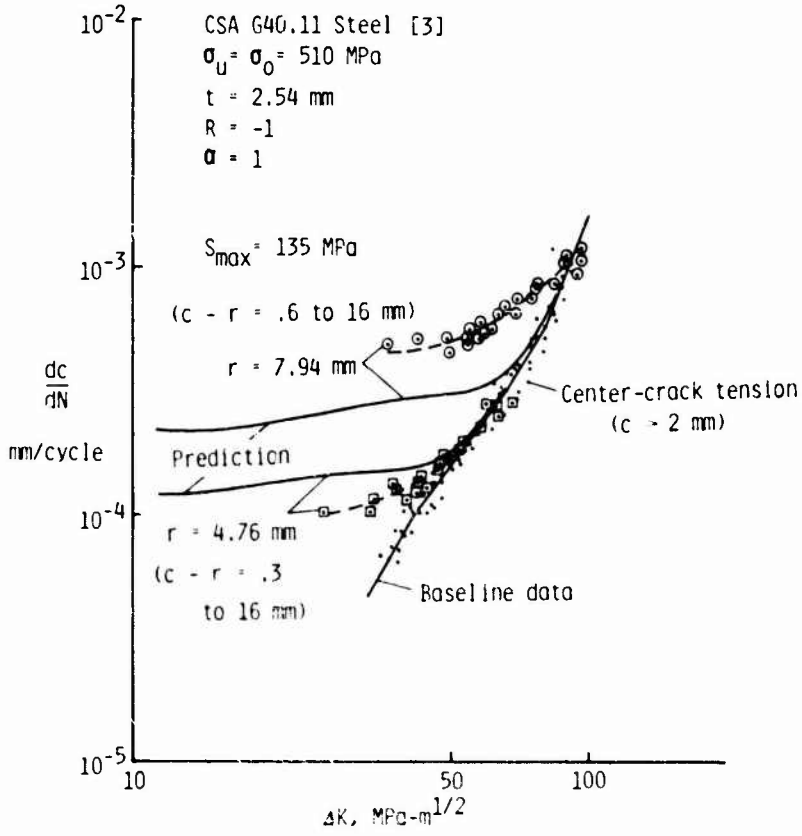

Figure 14.- Comparison of experimental and predicted crack-growth rates for small cracks emanating from a circular hole in steel specimens.

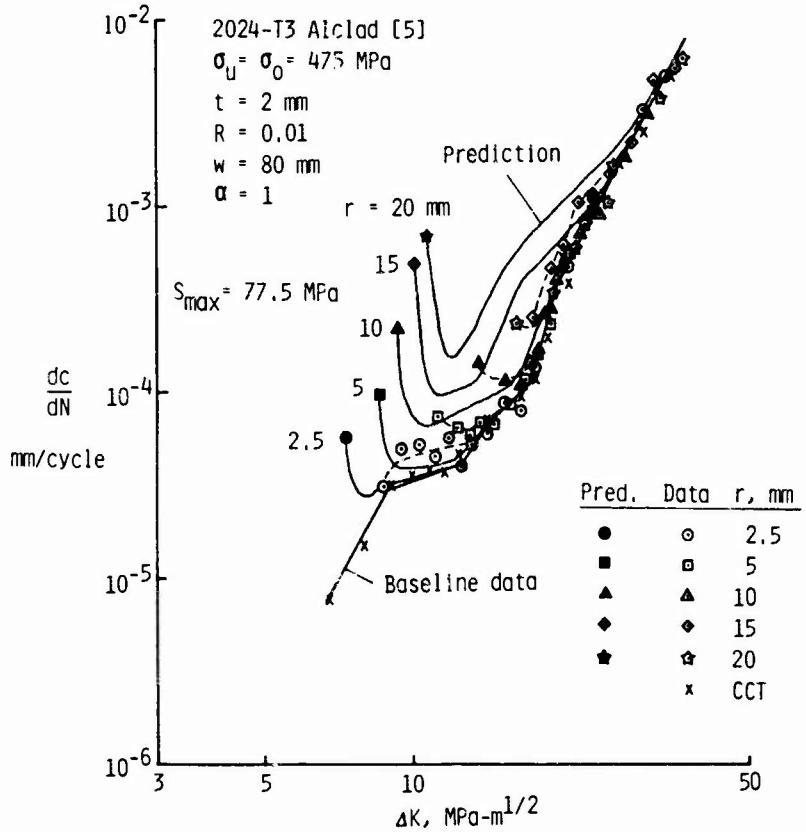

Figure 15.- Comparison of experimental and predicted crack-growth rates for small cracks emanating from a circular hole in aluminum specimens.

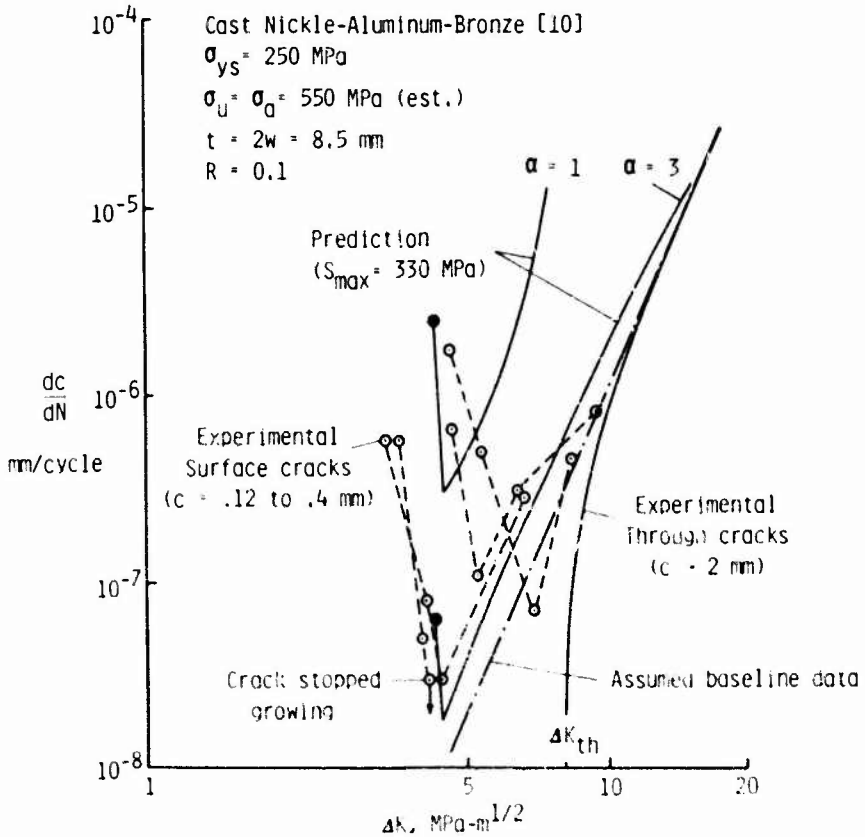

Figure 16.- Comparison of experimental and predicted crack-growth rates for small surface cracks in specimens subjected to a high stress level.

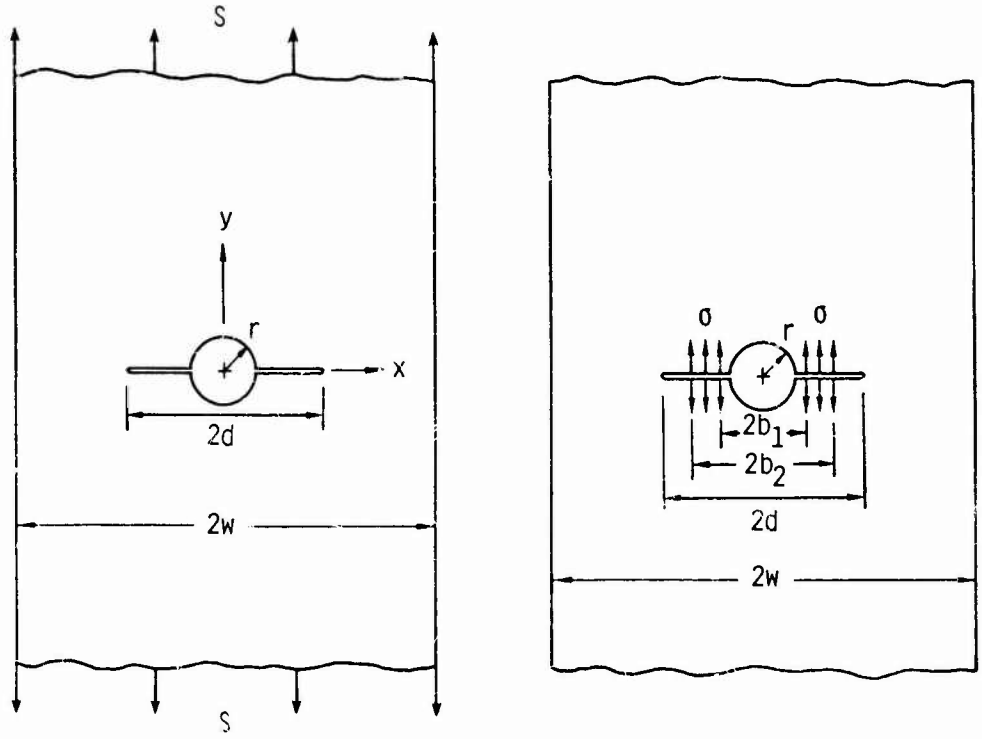

(a) Uniform stress (b) Partially-loaded crack

Figure 17.- Cracks from a hole in finite-width plate subjected to various loading.

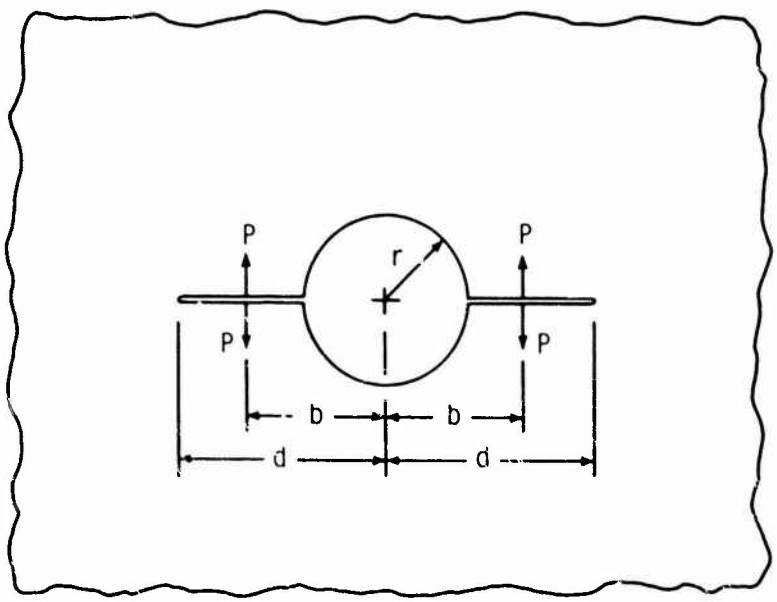

Figure 18.- Cracks from circular hole in infinite plate subjected to concentrated forces on crack surface.

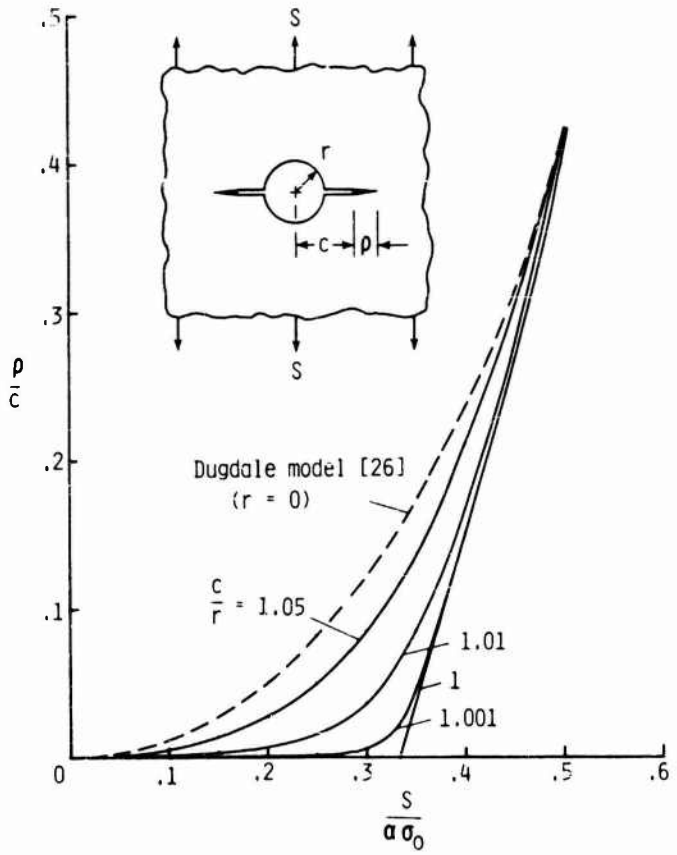

Figure 19.- Dugdale plastic-zone sizes for cracks from hole in an infinite plate subjected to remote uniform stress.